A translatable RNAi-driven gene therapy silences *PMP22/Pmp22* genes and improves neuropathy in CMT1A mice

Marina Stavrou, … , Scott Q. Harper, Kleopas A. Kleopa

Research   In-Press Preview   Neuroscience   Therapeutics

Charcot-Marie-Tooth disease type 1A (CMT1A), the most common inherited demyelinating peripheral neuropathy, is caused by *PMP22* gene duplication. Over-expression of wild-type PMP22 in Schwann cells destabilizes the myelin sheath, leading to demyelination and ultimately to secondary axonal loss and disability. No treatments currently exist that modify the disease course. The most direct route to CMT1A therapy will involve reducing PMP22 to normal levels. To accomplish this, we developed a gene therapy strategy to reduce *PMP22* using novel artificial microRNAs targeting human and mouse *PMP22/Pmp22* mRNAs. Our lead therapeutic microRNA, miR871, was packaged into an AAV9 vector and delivered by lumbar intrathecal injection into C61-het mice, a model of CMT1A. AAV9-miR871 efficiently transduced Schwann cells in C61-het peripheral nerves and reduced human and mouse *PMP22/Pmp22* mRNA and protein levels. Treatment at early and late stages of the disease significantly improved multiple functional outcome measures and nerve conduction velocities. Furthermore, myelin pathology in lumbar roots and femoral motor nerves was ameliorated. Treated mice also showed reductions in circulating biomarkers of CMT1A. Taken together, our data demonstrate that AAV9-miR871-driven silencing of PMP22 rescues a CMT1A model and provides proof of principle for treating CMT1A using a translatable gene therapy approach.

Find the latest version:

https://jci.me/159814/pdf

1   **TITLE PAGE**

2

3   **A translatable RNAi-driven gene therapy silences *PMP22/Pmp22* genes and**

4   **improves neuropathy in CMT1A mice**

5

6   **Authors:** **Marina Stavrou**[1], Alexia Kagiava[1], Sarah G. Choudury[2], Matthew J. Jennings[3],

7   Lindsay M. Wallace[2], Allison M. Fowler[2], Amanda Heslegrave[4,6], Jan Richter[5], Christina

8   Tryfonos[5], Christina Christodoulou[5], Henrik Zetterberg[4,6,7,8,9], Rita Horvath[3], Scott Q.

9   Harper[2,10] and Kleopas A. Kleopa[1, 11]*

10

11   [1]Neuroscience Department, The Cyprus Institute of Neurology and Genetics; Nicosia, Cyprus.

12   [2]Center for Gene Therapy, The Abigail Wexner Research Institute at Nationwide Children's

13   Hospital; Columbus, Ohio, USA.

14   [3]Department of Clinical Neurosciences, University of Cambridge; Cambridge, United

15   Kingdom.

16   [4]Department of Neurodegenerative Disease, UCL Institute of Neurology; London, United

17   Kingdom.

18   [5]Molecular Virology Laboratory, The Cyprus Institute of Neurology and Genetics; Nicosia,

19   Cyprus.

20   [6]UK Dementia Research Institute at UCL; London, United Kingdom.

21   [7]Department of Psychiatry and Neurochemistry, Institute of Neuroscience and Physiology, the

22   Sahlgrenska Academy at the University of Gothenburg; Mölndal, Sweden.

23   [8]Clinical Neurochemistry Laboratory, Sahlgrenska University Hospital; Mölndal, Sweden.

24   [9]Hong Kong Center for Neurodegenerative Diseases, Hong Kong, China

25 [10]Department of Pediatrics, The Ohio State University School of Medicine; Columbus, Ohio,

26 USA.

27 [11]Center for Neuromuscular Disorders, The Cyprus Institute of Neurology and Genetics;

28 Nicosia, Cyprus.

29

30 **Correspondence should be addressed to:** Prof. Kleopas A. Kleopa, MD, FAAN, FEAN

The Cyprus Institute of Neurology and Genetics

6 Iroon Avenue, P.O. Box 23462,

1683, Nicosia, Cyprus

Tel: +357 22 358600

Fax: +357 22 392786

kleopa@cing.ac.cy

31

32 **Short title**: Gene therapy for CMT1A demyelinating neuropathy

33 **ABSTRACT**

34

35 Charcot-Marie-Tooth disease type 1A (CMT1A), the most common inherited demyelinating

36 peripheral neuropathy, is caused by *PMP22* gene duplication. Over-expression of wild-type

37 PMP22 in Schwann cells destabilizes the myelin sheath, leading to demyelination and

38 ultimately to secondary axonal loss and disability. No treatments currently exist that modify

39 the disease course. The most direct route to CMT1A therapy will involve reducing PMP22 to

40 normal levels. To accomplish this, we developed a gene therapy strategy to reduce *PMP22*

41 using novel artificial microRNAs targeting human and mouse *PMP22/Pmp22* mRNAs. Our

42 lead therapeutic microRNA, miR871, was packaged into an AAV9 vector and delivered by

43 lumbar intrathecal injection into C61-het mice, a model of CMT1A. AAV9-miR871 efficiently

44 transduced Schwann cells in C61-het peripheral nerves and reduced human and mouse

45 *PMP22/Pmp22* mRNA and protein levels. Treatment at early and late stages of the disease

46 significantly improved multiple functional outcome measures and nerve conduction velocities.

47 Furthermore, myelin pathology in lumbar roots and femoral motor nerves was ameliorated.

48 Treated mice also showed reductions in circulating biomarkers of CMT1A. Taken together,

49 our data demonstrate that AAV9-miR871-driven silencing of PMP22 rescues a CMT1A model

50 and provides proof of principle for treating CMT1A using a translatable gene therapy approach.

51

52

53 **KEYWORDS**

54 CMT1A, inherited neuropathy, *PMP22*, gene silencing, miRNA, demyelination, AAV

55 vectors, gene therapy, Schwann cells.

56 **INTRODUCTION**

57

58   Charcot-Marie-Tooth disease (CMT) includes a genetically heterogeneous group of

59 inherited peripheral neuropathies with a prevalence of up to 1 in 2500 (1, 2). The autosomal

60 dominant demyelinating CMT neuropathy type 1A (CMT1A [MIM 118220]) is the most

61 common type, accounting for more than 50% of all CMT cases and resulting from an intra-

62 chromosomal duplication spanning 1.4 Mb on human chromosome 17p12 (3). The responsible

63 disease gene (*PMP22*) encodes the peripheral myelin protein of 22 kDa (PMP22), which is

64 located within this duplicated region (4-7). Patients with CMT1A develop distal muscle

65 weakness and atrophy, sensory loss, and absent reflexes, with typical onset at adolescence.

66 CMT1A is slowly progressive with marked variability in disease severity (8, 9). Sensory

67 responses are usually absent while motor nerve conduction velocities (MNCVs) are slowed,

68 ranging from 5 to 35 m/s in the forearm, but most average around 20 m/s, with uniform and

69 symmetric findings in different nerves. Although NCVs do not change significantly over

70 decades, motor amplitudes and the number of motor units decrease slowly, reflecting axonal

71 loss and correlating with progressive clinical disability.

72

73   PMP22 is mainly expressed by myelinating Schwann cells (SCs) and localized in

74 compact myelin (10), but is also present in non-neural cell types such as fibroblasts, endothelia,

75 and epithelia (11). Mouse studies support that PMP22 is normally involved in early steps of

76 myelin formation and in the maintenance of myelin and axons in the peripheral nervous system

77 (PNS) (12-15). In humans, *PMP22* mRNA and PMP22 protein overexpression in CMT1A

78 patient nerve biopsies indicates that increased PMP22 dosage is the most likely disease

79 mechanism underlying CMT1A (16-19). This hypothesis is further supported by recapitulation

80 of numerous CMT1A-associated phenotypes in PMP22 over-expressing rodent models (20-30),

81   including C61-het mice (22), which contain 4 copies of wild-type human *PMP22* on a normal

82   mouse background. The exact mechanisms by which PMP22 overexpression causes CMT1A

83   remain unclear but may involve proteasome dysfunction related to excessive amounts of PMP22

84   protein. Specifically, in normal myelinating and non-myelinating SCs, approximately 20% of

85   newly synthesized PMP22 is glycosylated while the remaining ~80% is targeted for proteasomal

86   endoplasmic reticulum-associated degradation (ERAD) (31). Thus, in CMT1A, over-expressed

87   PMP22 is thought to accumulate in perinuclear aggresomes (32, 33) and impair overall

88   proteasome activity (34), resulting in myelin sheath destabilization in SCs, and ultimately nerve

89   dysfunction.

90

91   Based on this model, the most direct approach to CMT1A therapy will likely involve

92   reducing over-expressed PMP22 to normal levels in SCs. Prior attempts to accomplish this

93   using drug-based approaches were unsuccessful in human clinical trials (NCT00484510,

94   NCT02600286, NCT05092841, NCT04762758, NCT03023540), and to date CMT1A remains

95   intractable. Nevertheless, progress continues in the field, with prospective adjunct therapies

96   approaching clinical trials (35-37), and several pre-clinical strategies to silence PMP22 reported

97   (38-61). For example, CRISPR/Cas9 was employed to directly target the *PMP22* gene by

98   deleting its regulatory regions with encouraging results *in vitro* (62) and *in vivo* (63), and

99   oligonucleotides have been tested to inhibit *PMP22* via promoter disruption or through mRNA

100   degradation using RNAase H or RNA-interference (RNAi)-based mechanisms (using DNA

101   gapmers or siRNAs, respectively) in different CMT1A rodent models (64-67). Among these

102   various silencing approaches, RNAi has so far been used most often as a prospective mechanism

103   to develop a CMT1A therapy (68).

104

105   RNAi is a conserved process of gene silencing triggered by endogenous miRNAs, which

106   are encoded in the genomes of eukaryotic organisms. Mature forms of natural miRNAs are

107   small (approximately 22 nucleotides long), non-coding RNA molecules that negatively regulate

108   the expression of a vast fraction of the transcriptome at the post-transcriptional level (69, 70).

109   Importantly, natural miRNAs can be modified in the form of siRNAs, shRNAs or artificial

110   miRNAs and re-targeted to specifically base-pair with disease genes, triggering target mRNA

111   degradation through the RNA-induced silencing complex (RISC). siRNAs are chemically

112   synthesized, produce transient effects, and require repeated, lifelong administration to achieve

113   long-term gene silencing. In contrast, shRNAs or artificial miRNAs can be cloned as DNA

114   expression cassettes, delivered to target cells within viral vectors, and can be transcribed *in vivo*

115   to produce long-term target gene silencing after one administration. As mentioned, siRNAs

116   have been used to trigger RNAi against *PMP22* in at least 3 published studies (65, 67), but RNAi

117   treatment of CMT1A *in vivo* and *in vitro* models was also achieved using gene therapy vectors

118   expressing natural microRNAs (mir-29a (71) or mir-318 (72)) or by an intraneurally injected

119   AAV2/9 vector expressing rodent *Pmp22*-targeting artificial shRNAs (73). These shRNAs

120   contain mismatches with the human *PMP22* sequence and were not tested in models expressing

121   human *PMP22*, so it is unclear if these sequences, as well as the invasive and laborious

122   intraneural injection method, can be translated to humans (73).

123

124   Here, we designed and tested a translatable AAV9-based gene therapy approach for

125   CMT1A using a novel artificial miRNA targeting conserved regions on the human *PMP22* and

126   mouse *Pmp22* transcripts. We demonstrate long-lasting therapeutic effects following a single,

127   clinically relevant lumbar intrathecal injection in a mouse model of CMT1A that expresses both

128   human and mouse *PMP22/Pmp22* gene products. Thus, our study provides proof-of-principle

129   for treating CMT1A with a gene therapy approach that uses artificial miRNA sequences and a

130   route of administration that can be translated to human trials.

131

132   **RESULTS**

133

134   **Design and *in vitro* validation of artificial miRNAs to downregulate human and murine**

135   ***PMP22.*** Full-length human *PMP22* and mouse *Pmp22* are encoded by 5 exons, with two

136   alternatively spliced first exons containing 5' UTR sequences (ex1* 1a and ex1b). Both

137   variants, encode identical 483 base-pair open reading frames and share the same 3' UTR, which

138   is located in exon 5 (ex5) (ORFs) (**Figure 1A**). To ensure we targeted all *PMP22* transcripts,

139   we excluded exon 1 from the query sequence and designed artificial miRNAs targeting human

140   *PMP22* exons 2-5 (1,655 nucleotides) using a previously described algorithm (74). This screen

141   identified 117 candidates. Because we intended to use the RNA polymerase III (pol III)-

142   dependent U6 promoter to drive miRNA expression, we excluded 29 of the 117 candidates due

143   to the presence of RNA pol III termination sequences (5-6 T's) within the miRNA expression

144   cassettes. The remaining 88 sequences were additionally filtered to ensure the antisense guide

145   strand of the miRPMP22 miRNAs would equally target human and mouse *PMP22/Pmp22*

146   sequences. Only 8 sequences (9%) showed this conservation, and all were located in exon 5,

147   which encodes 3' UTR (**Figure 1A**). Following cloning into a U6T6 expression plasmid, we

148   empirically tested all 8 miRPMP22 miRNAs (miR868, miR869, miR871, miR872, miR1706,

149   miR1740, miR1741, miR1834) for silencing efficacy (**Figure 1B to C and Supplemental**

150   **Figure S1**). Specifically, we co-transfected HEK293 cells with each individual U6-miRPMP22

151   plasmid and CMV-driven hu*PMP22* or mu*Pmp22* full-length cDNAs, then harvested RNA 24

152   hours later, generated cDNA and performed RT-qPCR using for hu*PMP22* or mu*Pmp22*,

153   normalized to hu*RPL13A*. Negative controls included cells transfected with *PMP22/Pmp22*

154 and U6.miRGFP (miRNA targeting EGFP) or an empty U6T6 plasmid (no miR). Data were

155 collected and averaged from three independent experiments, with each RT-qPCR assay

156 performed in triplicate. Although 7 of 8 miRPMP22s (87.5%) showed some level of silencing

157 compared to the "no miR" control, only miR868 and miR871 showed statistically significant

158 silencing of hu*PMP22* and mu*Pmp22* sequences. Because miR871 consistently silenced both

159 genes ~60%, we chose the miR871 sequence as our lead. The U6-miR871 sequence was then

160 cloned into a self-complementary AAV (scAAV.CMV.EGFP) backbone containing a separate

161 CMV.EGFP reporter gene, and we generated AAV9 particles using triple transfection in

162 HEK293 cells (hereafter referred to as AAV9-miR871). Lysates were purified by iodixanol

163 gradient ultracentrifugation and FPLC, as previously described (75). Similarly, we generated a

164 control scAAV9.CMV.EGFP vector expressing a U6 promoter-driven miRNA targeting *E. coli*

165 *LacZ* gene (hereafter referred to as AAV9-miRLacZ).

166

167 **Biodistribution and expression following lumbar intrathecal injection of AAV9-miR871.**

168 We delivered AAV9-miR871 vector expressing the EGFP gene under the CMV promoter into

169 2-month-old C61 heterozygous mice (22) (hereafter referred to as CMT1A mouse) using

170 lumbar intrathecal injection (20 μl containing a total of 5e11vg/mouse). At 6-weeks post

171 injection we examined AAV9-miR871 biodistribution and transduction in PNS cells. For this

172 purpose, we employed vector genome copy numbers (VGCNs) and EGFP expression analysis

173 in anterior lumbar roots, sciatic and femoral nerves. EGFP was detected as auto-fluorescence

174 in the perinuclear cytoplasm of a subset of PNS cells as well as in the axons of lumbar roots,

175 sciatic and femoral nerves (**Figure 2A**). The percentage of EGFP expressing SCs in

176 immunostained tissue sections reached an average of 54.78%±4.53 in anterior lumbar roots,

177 44.07%±2.96 in sciatic nerves and 40.18%±4.93 in femoral nerves (n=4 mice; **Fig. 2B**).

178   VGCNs in DNA extracted from PNS tissues reached 2.44 in anterior lumbar roots, 1.23 in

179   sciatic nerve and 0.69 in femoral nerve (n=4 mice; **Figure 2C**).

180

181   ***In vivo* validation of AAV9-miR871-mediated silencing of *PMP22* gene in CMT1A mice.**

182   Prior to any treatment studies, we performed a detailed characterisation of baseline functional

183   and morphological deficits of the C61-het CMT1A mouse line, which contains four copies of

184   the human *PMP22* gene and 2 normal copies of mouse *Pmp22*, compared to wild type (WT)

185   mice at 2, 4, 6, 8, and 10 months of age. We confirmed progressive functional impairment

186   associated with early onset demyelination (**Supplemental Figures S2 to S7**). We also assessed

187   the potential toxicity of AAV9-miRLacZ vector after injection into 2-months-old CMT1A

188   mice that were examined 6 weeks (3.5-months-old) or 4 months (6-months-old) later. AAV9-

189   miRLacZ caused no significant increase in the numbers of inflammatory cells in spinal roots,

190   sciatic nerves, or dorsal root ganglia (DRGs) beyond the baseline (**Supplemental Figures S8,**

191   **S9, S11**). However, injection of AAV9-miRLacZ increased the number of CD20 and CD3

192   positive cells in CMT1A mouse livers 6-weeks after injection (3.5-months-old) but this

193   reaction subsided by the 4-months post-injection time point (6-months-old) (**Supplemental**

194   **Figure S10**). Interestingly, inflammatory infiltrates increased with age in the PNS of non-

195   injected CMT1A mice (**Supplemental Figures S8 to S9**).

196

197   After we confirmed sufficient biodistribution, transduction of PNS tissues and safety,

198   we evaluated the efficacy of AAV9-miR871 to silence *PMP22/Pmp22* gene expression and

199   reduce overall PMP22/Pmp22 protein levels, compared to the expression of other myelin-

200   related genes and proteins. We injected AAV9-miR871, which targets both the hu*PMP22* and

201   mu*Pmp22* transcript, or the AAV9-miRLacZ negative control, which expresses a functional

202   but non-targeting miRNA, into adult CMT1A mice and then analysed gene expression by real-

203   time PCR and western blot at 6 weeks post-injection. At the mRNA level, AAV9-miR871

204   downregulated hu*PMP22* and mu*Pmp22* in spinal roots, sciatic and femoral nerves, whereas

205   other myelin-related genes were mostly elevated (**Figure 2D to E and Supplemental Table**

206   **S1**). The mu*Gjb1* transcript levels were increased in all tissues examined. The mu*Mpz* and *Gldn*

207   transcript levels were elevated only in roots while the mu*Cnp* transcript levels were elevated

208   only in sciatic nerves. At the protein level, AAV9-miR871 selectively reduced huPMP22 levels

209   in all PNS tissues examined (in roots: -66%, sciatic nerve: -86%, femoral nerve: -64%),

210   whereas muMpz protein levels were increased in roots (by 23%) and femoral nerves (by 34%).

211

212   **Early treatment of CMT1A mice.** After validating AAV9-miR871 *in vivo* PNS

213   biodistribution and *PMP22/Pmp22* gene silencing efficacy, we proceeded with a proof-of-

214   concept treatment trial at early stages of the neuropathy in the CMT1A mouse model. Two-

215   month-old CMT1A mice were injected with either AAV9-miR871 or -miRLacZ and evaluated

216   at 4 months post-injection. For outcome analysis we included *PMP22/Pmp22* expression levels

217   using real-time PCR and western blot, behavioural testing, circulating neurofilament light (NF-

218   L) and growth differentiation factor 15 (Gdf15) quantification, electrophysiological

219   examination, as well as morphometric analysis of myelination in semithin sections and

220   evaluation of inflammatory infiltrates in the PNS by immunohistochemistry (**Figures 3 to 5**).

221   We confirmed adequate biodistribution by VGCN measurement in PNS and non-PNS tissues

222   as well as by immunofluorescence analysis in lumbar roots and sciatic nerves (**Supplemental**

223   **Figure S12**).

224

225   At the mRNA level, early treatment with AAV9-miR871 in CMT1A mice

226   downregulated hu*PMP22* and mu*Pmp22* in roots, and sciatic and femoral nerves, while also

227   elevating mu*Mpz,* mu*Cnp,* mu*Gldn and* mu*Gjb1* transcripts levels (**Figure 3B to C and**

228 **Supplemental Table S2**). At the protein level, early treatment with AAV9-miR871 in CMT1A

229 mice reduced huPMP22 and muPmp22 levels in spinal roots (-43% huPMP22, -45%

230 muPMP22), sciatic (-51% huPMP22, -74% muPMP22) and femoral nerves (-87% huPMP22,

231 -38% muPMP22) (**Figure 3D to I**). In contrast, muMPZ protein levels were increased in roots

232 (63%) and femoral nerves (102%) reflecting improved myelination, while they remained

233 unchanged in sciatic nerves (**Figure 3D to I**).

234

235 We assessed motor performance in all groups before injection and until the end of the

236 observation period by rotarod (5 and 17.5 rpm), grip and hang test analysis (**Figure 3J to M**

237 **and Supplemental Figure S13**). Time course analysis of the above tests showed that AAV9-

238 miR871 treatment improved motor performance of CMT1A mice reaching WT levels, while

239 AAV9-miRLacZ treated CMT1A mice performed similar to non-injected CMT1A mice and

240 significantly worse than WT mice (**Figure 3J to M and Supplemental Figure S13**).

241 Moreover, AAV9-miR871 early treatment rescued completely the hindlimb clasping

242 phenotype of CMT1A mice (**Figure 3N and Supplemental Figure S14**).

243

244 Electrophysiological examination in 6-month-old mice (4 months after vector injection)

245 (**Figure 3O to P**) showed that MNCV score was significantly improved in AAV9-miR871

246 treated mice (36.87±5.60 m/s) compared to the AAV9-miRLacZ group (25.89±1.99 m/s),

247 approaching WT values at the same age (41.61±5.06m/s). Although the amplitude of the

248 compound muscle action potential (CMAP) was also significantly improved in treated mice

249 (3.52±1.08 mV) compared to AAV9-miRLacZ controls (1.44±0.59 mV), it did not reach WT

250 levels (6.89±1.76 mV).

251

252   Similar to other CMT blood biomarkers studies, we found that circulating NF-L (76-

253   79) and Gdf15 (80, 81) levels, associated with axonal degeneration, were significantly

254   ameliorated after early treatment of CMT1A mice with AAV9-miR871 (NF-L: 321.37±51.68

255   pg/ml, Gdf15: 56.25±14.84 pg/ml) compared to AAV9-miRLacZ vector-treated littermates

256   (540.65±134.49 pg/ml, Gdf15: 81.93±23.12 pg/ml) (**Figure 3Q to R**). This reduction of NF-L

257   and Gdf15 levels in the AAV9-miR871 treatment group is consistent with improved motor

258   function following gene silencing treatment. Thus, NF-L and Gdf15 blood levels may be useful

259   as treatment-responsive and clinically relevant biomarkers for future gene therapy in CMT1A

260   patients.

261

262   We performed morphometric analysis of myelination in transverse semithin sections of

263   anterior lumbar roots and femoral motor nerves of 6-month-old CMT1A mice injected at the

264   age of 2 months with either the AAV9-miR871 or the AAV9-miRLacZ vector. We examined

265   multiple roots and bilateral femoral motor nerves from each mouse and calculated the

266   percentage of thinly myelinated and demyelinated fibers, as well as the number of onion bulb

267   formations. In both roots (**Figure 4A to E**) and femoral nerves (**Figure 4F to J**) the percentage

268   of thinly myelinated and demyelinated fibers was significantly reduced in treated mice. Spinal

269   roots also showed reduced numbers of onion bulb formations while femoral onion bulb

270   formations were already low at baseline and not altered after treatment. The degree of myelin

271   pathology was too mild in sciatic nerves of CMT1A mice to be considered as a treatment

272   readout (**Supplemental Figure S15**).

273

274   Finally, for this early treatment group, we employed immunofluorescence analysis to

275   evaluate the inflammatory status of lumbar roots and sciatic nerves (**Figure 5 and**

276   **Supplemental Figures S16 to S18**). AAV9-miR871 treatment decreased the percentage of

277   CD20, CD45, CD68 and CD3 positive cells. Moreover, injection with the therapeutic vector

278   did not cause any inflammatory responses in the liver at 4-months post injection

279   (**Supplemental Figure S18**).

280

281   **Late treatment compared to extended early treatment.** After assessing the effectiveness of

282   early treatment with AAV9-miR871 in CMT1A mice, we further examined its effectiveness

283   when injected later in the disease course. We injected mice either at 6 months (late treatment)

284   or at 2 months of age (extended early treatment) and analyzed various outcomes at 10 months

285   of age. We evaluated both late treated mice (at 4 months post-injection) and extended early

286   treated mice (at 8 months post-injection) using VGCN calculation, behavioural testing, blood

287   NF-L and Gdf15 testing, electrophysiological examination, as well as by morphometric

288   analysis of myelination and immunohistochemistry, while real-time PCR and western blot

289   analysis were performed only in late treated groups (**Figure 6A**). Vector biodistribution in

290   older animals was confirmed by VGCN in PNS and non-PNS tissues (**Supplemental Figures**

291   **S19A and S20**). In late treated group, we confirmed vector biodistribution with EGFP

292   expression rates in lumbar roots and sciatic nerves (**Supplemental Figure S19B**).

293

294   At the mRNA level, as in early treatment, late treatment with AAV9-miR871 in

295   CMT1A mice downregulated hu*PMP22* and mu*Pmp22* while also elevating mu*Mpz,* mu*Cnp,*

296   mu*Gldn* and mu*Gjb1* transcripts levels in roots, sciatic and femoral nerves (**Figure 6B to C**

297   **and Supplemental Table S3**). At the protein level, late treatment with AAV9-miR871 reduced

298   huPMP22 and muPmp22 in all PNS tissue samples examined (**Figure 6D to I**). In contrast,

299   muMPZ protein levels were increased in roots and femoral nerves reflecting improved

300   myelination, but remained unchanged in sciatic nerves (**Figure 6D to I**).

301

302   We compared motor performance of the late treatment group to extended early

303   treatment and age-matched non-injected WT and CMT1A mice (**Figure 6J to N and**

304   **Supplemental Figures S21 to S22**). We evaluated all groups before injection and until the end

305   of the observation period by rotarod at 5 rpm and 17.5 rpm, grip strength and hang test analysis

306   (**Figure 5J to M**). Time course analysis of the above tests showed that late and extended early

307   AAV9-miR871 treated CMT1A mice performed similarly reaching WT levels, while AAV9-

308   miRLacZ late treated CMT1A mice performed similar to non-injected CMT1A mice and

309   significantly worse than WT mice (**Figure 6J to M and Supplemental Figures S21 to S22**).

310   AAV9-miR871 late treatment improved the hindlimb clasping phenotype of CMT1A mice but

311   without reaching WT levels, in contrast to extended-early treated mice in which the phenotype

312   was totally rescued reaching WT levels (**Figure 6N and Supplemental Figure S23**).

313

314   Electrophysiological examination in 10-month-old mice showed that sciatic MNCV

315   was significantly improved in both late (36.92 ± 3.94 m/s) and extended-early (38.74 ± 5.30 m/s)

316   AAV9-miR871 treated CMT1A mice compared to the AAV9-miRLacZ group (24.82 ± 2.58

317   m/s) (**Figure 6O**). Interestingly, only extended early treated CMT1A mice reached age-

318   matched WT values (43.50 ± 2.72 m/s). CMAP amplitudes were not improved in any of the

319   AAV9-miR871 treatment groups (**Figure 6P**). Similarly, NF-L and Gdf15 levels remained

320   elevated in late-treated animals compared to age-matched WT mice (**Figure 6Q to R**).

321

322   We performed morphometric analysis of myelination in transverse semithin sections of

323   PNS tissues of 10-month-old late and extended early treated CMT1A mice. With this analysis,

324   we showed that anterior lumbar roots (**Figure 7A to F**) and femoral motor nerves (**Figure 7G**

325   **to L**) present significantly reduced percentages of thinly myelinated and demyelinated fibers

326   in late treated mice but without reaching WT levels. In contrast, these morphological

327   abnormalities were fully rescued in extended-early treated mice reaching WT levels (**Figure**

328   **7A to L**). The degree of myelin pathology remained too mild in sciatic nerves of 10-month-old

329   CMT1A mice to be considered as a treatment readout (**Supplemental Figure S24**).

330

331   As in the early treatment group, analysis of inflammation by immunofluorescence

332   revealed that late treatment with AAV9-miR871 decreased the numbers of CD20, CD45, CD68

333   and CD3 positive cells in PNS tissues (**Figure 8 and Supplemental Figures S25 to 26**).

334   Injection with the therapeutic vector did not cause any inflammatory responses in the liver at

335   4-months post injection (**Supplemental Figure S27**).

336

337   **DISCUSSION**

338

339   CMT1A is the most common inherited demyelinating neuropathy, resulting from a

340   *PMP22* gene dosage effect in SCs. Ideally, CMT1A therapies should reduce over-expressed

341   *PMP22* while avoiding excessive knockdown that could lead to the milder phenotype of

342   hereditary neuropathy with pressure palsies (HNPP). We accomplished that here with our study

343   presenting the first translatable AAV9-mediated *PMP22* gene silencing approach leading to

344   phenotypic improvement in a CMT1A mouse model. Although this is a pre-clinical study, we

345   designed our approach from the outset with an eye toward translation to prospective human

346   clinical trials, in two ways. First, the therapeutic construct is applicable to animal models and

347   human CMT1A patients alike. The most relevant animal models, like the C61-het mouse we

348   used here, express transgenic copies of human PMP22 on a normal mouse background. Thus,

349   both mouse and human *Pmp22/PMP22* genes contribute to excessive gene dosage leading to

350   CMT1A-like phenotypes, and testing a translatable approach in mice requires targeting both

351   transcripts. Importantly, the artificial microRNA we designed, miR871, targets both human

352   *PMP22* and murine *Pmp22* transcripts. Second, we delivered AAV9-miR871 through a

353   clinically applicable lumbar intrathecal injection method into the C61-het CMT1A model,

354   which reproduces the clinical course, severity and symptoms of CMT1A patients.

355

356   The translatability and effectiveness of the intrathecal administration route has been

357   demonstrated in bigger animals (82, 83) and in human trials (NCT03381729, NCT02362438)

358   that showed effects in nerves distal to the injection site, including transduction of SCs in the

359   tibial nerve of dogs after intrathecal injection of AAV9 (83). Another route of administration

360   that could be easily translated in the clinic is the intravenous injections. However, our studies

361   in mice showed that intrathecal injection provides adequate biodistribution throughout the PNS

362   with much lower vector amounts injected compared to intravenous delivery (84). Intraneural

363   injections of AAV.shRNA were also proposed to treat a CMT1A model (73), however the

364   translatability of this delivery method is considered challenging in the clinic.

365

366   In addition to incorporating species conservation and a feasible route of administration

367   into our study design, we also demonstrated efficacy at multiple levels. First, we confirmed *in*

368   *vitro* and *in vivo* the *PMP22/Pmp22* silencing efficiency of miR871 and its effects on other

369   myelin related genes and proteins, while also assessing the transduction efficiency of AAV9 in

370   PNS tissues after lumbar intrathecal injection (**Figures 1 to 2**). We then demonstrated by

371   multiple outcome measures the therapeutic effects of AAV9-miR871 after treatment both at

372   early and later stages of the neuropathy, supporting the relevance of this approach for direct

373   clinical translation to treat CMT1A. As demonstrated through our detailed baseline

374   longitudinal functional and morphological analysis, the C61 het model of CMT1A used in this

375   study develops an early onset, progressive demyelinating pathology that reproduces human

376   disease features (**Supplemental Figures S2 to S7**). Thus, already at the early intervention time

377   point, the model presented significant pathological features and slowing of nerve conduction

378   velocities that progressed with aging. Therefore, both early and late treatments represent post-

379   onset interventions, reproducing the clinical scenario of treating younger or older patients

380   suffering from CMT1A, in whom demyelination is already present in childhood (85, 86),

381   followed by slowly progressive axonal loss (8, 9, 87, 88). Our mouse data suggest that earlier

382   treatment is effective, as several outcome measures were corrected to wild-type levels (**Figures**

383   **3 to 5**). Direct comparison of extended early- and late- treated CMT1A mice, injected at 2 or 6

384   months of age, respectively, and analysed at 10 months of age, confirmed that treatment more

385   efficiently reversed disease manifestations if given earlier (**Figures 6 to 7**). This could be

386   explained by the fact that later stages of the neuropathy are characterized by significant axonal

387   degeneration. While it appears feasible to stimulate re-myelination by transduced

388   demyelinating SCs, increasing axonal loss found at later stages is irreversible. Nevertheless,

389   our data suggest that the ability to impact CMT1A-like symptoms in mice with pre-existing

390   pathology is promising for translating this strategy to humans who may already be suffering

391   the effects of CMT1A. Indeed, our work is consistent with a tetracycline-inducible *Pmp22*

392   transgenic mouse study (89). *Pmp22* over-expression occurred in the absence of tetracycline,

393   causing demyelination and numerous neuropathic phenotypes. Importantly, when mice were

394   given tetracycline, thereby shutting off the Pmp22 transgene, myelin normalization began

395   occurring within 1 week, with nearly normal myelin by 4 months. Together, these data and

396   ours suggest some CMT1A phenotypes may be reversible. It is also possible we may see even

397   greater reversal of phenotypes as mice age beyond 4 months post-treatment.

398

399   Another question we considered, regarding translation, was the necessity to restrict

400   miR871 expression to SCs alone. In our previous studies (84) we demonstrated that an AAV9

401   vector expressing a transgene through the SC specific *Mpz* promoter efficiently transduced

402 myelinating SCs throughout the PNS following a single lumbar intrathecal injection. In the

403 current study, we used AAV9 to deliver a U6.miR.CMV.EGFP construct in which both

404 sequences (EGFP and miR871) were driven by ubiquitous promoters (CMV and U6,

405 respectively) (**Figure 1D**). We calculated transduction rates via immunofluorescence using

406 the CMV.EGFP reporter gene and VGCN analysis (**Figure 2**). Not surprisingly, expression

407 was more widespread with both SCs and other cell types transduced, including motor and

408 sensory neurons, leading to axonal expression. We also detected VGCN in many non-PNS

409 tissues typically transduced by AAV9, with the highest being liver (**Supplemental Figures**

410 **S12, S19**), but without any apparent toxic effects in lumbar roots, sciatic nerves, liver and

411 DRGs (**Figure 5 and 8, Supplemental Figures S8 to S11, S16 to S18, S25 to S27**). Given

412 that PMP22 expression levels are normally very low and do not have any known effects in

413 other cell types besides myelinating SCs (11, 90-92), we do not expect any adverse effects by

414 ubiquitously silencing PMP22 expression. It is also important to mention that transduction

415 evaluation through a reporter gene may not directly correlate with miR expression, when using

416 two different ubiquitous promoters. An emerging area of study is the ability of miRs to travel

417 outside transduced cells through exosomes and potentially act at distant sites and neighbouring

418 cells. We did not directly measure exosome packaging of miR871, but future work should

419 determine the potential of incomplete transduction leading to broader correction in adjacent,

420 non-transduced cells.

421

422 The 5e11 vg/mouse vector dose used for intrathecal injection in this study corresponds

423 to ~2.3e13 vg/Kg. With this dose, we achieved sufficient SC transduction and PMP22 silencing

424 to improve molecular, histopathological, and functional deficits. As such, this dose is

425 comparable to those used in prior clinical AAV9 gene therapy studies that targeted motor

426 neurons in the spinal cord, including the Avexis SMA trial for intrathecal delivery of

427   Zolgensma 1.2e13vg/kg (93) (NCT03381729) and the giant axonal neuropathy (GAN) clinical

428   trial, where intrathecal doses ranged from 3.5e13 to 3.5e15 total vg/patient (~1.75e12 vg/kg -

429   1.75e13 vg/kg) (94) (NCT02362438). Given that our dose is slightly higher than the ones

430   currently used in clinical trials, and the fact that our potential treatment population will be

431   mostly adults with CMT1A, a dose escalation study would be useful in identifying the optimal

432   vector concentration that will provide robust therapeutic benefit, and minimal risk of *PMP22*

433   haploinsufficiency.

434

435   To examine the potential side effects of *PMP22/Pmp22* over-silencing, we tested

436   AAV9-miR871 in WT mice (**Supplemental Results and Figures S28 to S34**). Despite

437   muPmp22 levels being significantly reduced in WT-injected mice we found only mild

438   functional and electrophysiological abnormalities without the typical HNPP-like phenotype

439   (95). Since our treatment is not intended to be applied to individuals with normal levels of

440   PMP22 expression, the partial phenotype observed in WT mice based on the dual human-

441   murine targeting capacity of miR871 does not raise safety concerns regarding the potential

442   treatment of CMT1A patients. This set of experiments in WT mice also underscores the

443   importance of targeting all sources of *PMP22/Pmp22* in an animal model, especially when

444   performing dose-finding studies to identify potential clinical doses.

445

446   Several CMT1A therapeutic approaches have been suggested so far (61, 68) with the

447   most clinically advanced being oral PXT3003. Although, PXT3003 was shown to improve the

448   symptoms of CMT1A rats (56) and humans (60), its Pmp22 silencing efficiency was shown

449   only at the mRNA level in the rat overexpressing murine Pmp22. It is still unclear how

450   PXT3003 affects human PMP22. Although other pharmacological treatments have been

451   suggested through the years, most of them are symptomatic, require repeated treatment

452   sessions, or have potential long-term side effects. For example, intravenously delivered

453   squalenoyl siRNA PMP22 nanoparticles (67) have been shown to provide therapeutic benefit

454   in JP18/JY13 mice overexpressing human *PMP22* gene. However, potential toxicity with

455   repeated dosing and long-term stability, as well as effects of this treatment on *PMP22* mRNA

456   or protein levels remain to be shown. On the contrary, a gene therapy approach like ours would

457   provide a one-off treatment option. In a previously reported pre-clinical gene therapy approach,

458   AAV2/9 vectors expressed shRNAs specifically designed to target murine *Pmp22* (73).

459   Because the shRNAs contain potentially disruptive mismatches with the human transcript, their

460   direct translatability in humans was untested and remains unclear. Moreover, the shRNA

461   vectors were delivered through direct intraneural injection, a method that is more difficult to

462   translate into clinical practice for treating CMT1A, and bares more risks because of the toxic

463   nature of concentrated anesthesia and the risk of direct fiber damage (96). In contrast, the

464   lumbar intrathecal injection used in our study is considered a routine procedure that can be

465   easily applied in the clinic providing a widespread biodistribution in the PNS. Compared to

466   intravenous delivery, intrathecal delivery also requires a much lower viral volume to provide

467   beneficial effects and hence results in lower toxicity (84, 97). It remains to be shown that

468   adequate biodistribution can also be achieved in larger animals before clinical translation.

469

470   Regarding safety of AAV9-based vectors in humans, follow-up studies in AAV9-

471   treated SMA patients suggested stable beneficial effects from Zolgensma with no major

472   adverse reactions or long-term toxicity (93, 98, 99). However, more recent studies suggest that

473   long term overexpression of proteins (100) or microRNAs (101) via AAV9 viral vectors may

474   dysregulate endogenous mechanisms causing toxic side-effects. Our data suggested that

475   AAV9-miR871 treatment did not cause inflammation in PNS tissues, as had been previously

476   suggested in another study using the AAV9 serotype carrying a different payload (102), but in

477   fact acted to reduce inflammation native to the CMT1A animal model. Moreover, injection

478   with the therapeutic vector did not cause any chronic inflammatory responses in the liver at 4

479   months post injection (**Supplemental Figure S18 and S27**). Although our approach was

480   shown to improve the baseline inflammatory status of the CMT1A model without causing any

481   systemic or liver toxicity, it will be important to demonstrate its safety with more detailed

482   toxicity studies consistently across different species. Potential cellular and humoral immune

483   responses can be stimulated against the AAV capsid or protein-coding gene product. Since our

484   one-off therapeutic payload is a non-coding RNA, our vector should be inherently less

485   immunogenic than vectors used in gene replacement strategies.

486

487   For planning successful clinical trials in CMT1A it is important to establish relevant

488   and sensitive outcome measures. The gene silencing approach described here provides

489   functional improvements that can be easily evaluated in patients through electrophysiological

490   testing. Since previous clinical trials suggested lack of sensitivity of standard CMT clinical

491   scores to detect treatment response (45, 103), more detailed clinical functional and patient-

492   reported outcome measures will also be necessary (104-107), along with MRI-based

493   quantification of muscle atrophy (108). Here we also demonstrate for the first time the

494   responsiveness of NF-L (109, 110) and Gdf15 (80, 81) plasma biomarkers in a CMT1A model.

495   Responsiveness of these translatable biomarkers is highly encouraging for their utility in

496   parallel clinical trials of miRNA therapies. Although, a recent study (79) showed lack of

497   correlation of NF-L plasma levels with disease progression over time in CMT1A patients, this

498   might be due to the already progressed age of the patients tested (mean age: 46). In this regard,

499   validation of additional clinically relevant plasma and skin biomarkers as indicators for future

500   gene therapy efficacy would be essential (19, 111 , 112, 113).

501

502   **In conclusion**, we developed and characterized an artificial microRNA designed to

503   target specifically human *PMP22* and mouse *Pmp22* transcripts, and evaluated therapeutic

504   benefit in a CMT1A mouse model that reproduces CMT1A associated phenotypes. Our results

505   indicate that a single lumbar intrathecal injection of AAV9-miR871 at early and late stages of

506   the neuropathy and always post-onset, can correct the functional, morphological and

507   inflammatory abnormalities of CMT1A without causing any apparent side effects. Taken

508   together, these results constitute an important step towards the development of a clinically

509   relevant and translatable gene therapy to treat CMT1A.

510

511

MATERIALS AND METHODS

All materials and methods are presented in the **Supplemental data**.

Data and materials availability: All the data are present in the manuscript or in the Supplementary figures.

Statistical analysis: Each set of data is presented as the mean ± SD or SEM, with n equal to the number of biological repeats for *in vitro* experiments or independent samples from individual animals for *in vivo* experiments. For comparison of means between two independent groups, unpaired Student's t test was performed. For comparison of means between three or more independent groups one-way ANOVA was performed. Statistical significance for all experiments was defined as $P < 0.05$. When ANOVA tests suggested significant difference among groups, Tukey's multiple comparison post hoc test was applied. When a sample group was used for more than one comparison, Bonferroni correction of p-values was additionally applied. All statistical analyses were performed using GraphPad Prism v.6 software.

Study approval. All animal procedures were approved by the Cyprus Government's Chief Veterinary Officer (project license CY/EXP/PR.L3/2017) according to national law, which is harmonized with EU guidelines (EC Directive 86/609/EEC).

AUTHOR CONTRIBUTIONS

M.S. co-designed and conducted or directed all experiments, acquired data, analysed data, created figures and legends, drafted and reviewed the manuscript. A.K. performed electrophysiology experiments. S.G.C. performed and analysed *in vitro* screening of artificial microRNAs. M.J.J. and R.H. standardised, performed and analysed ELISA for serum Gdf15 levels. L.M.W. contributed to *in vitro* screening of artificial microRNAs. A.M.F. assisted with viral vector production. A.H. and H.Z. performed and analysed plasma NF-L levels. J.R, C.T. C.C. performed and analysed VGCN. S.Q.H designed artificial microRNAs and supervised *in*

537   *vitro* screening, created figures and legends, drafted and reviewed the manuscript. K.A.K. co-

538   designed and supervised all experiments, drafted and reviewed the manuscript. All authors read

539   and approved the final manuscript.

540

559

560

561

562 **COMPETING INTERESTS**

563 The sequences and methods described here were included in a provisional patent application

564 filed on December 1, 2020 (PCT/US21/61177). S.Q.H., K.A.K., and M.S. are listed as

565 inventors. H.Z. has served at scientific advisory boards and/or as a consultant for Abbvie,

566 Alector, Annexon, Artery Therapeutics, AZTherapies, CogRx, Denali, Eisai, Nervgen, Novo

567 Nordisk, Pinteon Therapeutics, Red Abbey Labs, Passage Bio, Roche, Samumed, Siemens

568 Healthineers, Triplet Therapeutics, and Wave, has given lectures in symposia sponsored by

569 Cellectricon, Fujirebio, Alzecure, Biogen, and Roche, and is a co-founder of Brain Biomarker

570 Solutions in Gothenburg AB (BBS), which is a part of the GU Ventures Incubator Program

571 (outside submitted work).

572

573 **REFERENCES**

574

575 1.   Skre, H. 1974. Genetic and clinical aspects of Charcot-Marie-Tooth's disease. *Clin*

576   *Genet* 6:98-118.

577 2.   Martyn, C.N., et al. 1997. Epidemiology of peripheral neuropathy. *J Neurol Neurosurg*

578   *Psychiatry* 62:310-318.

579 3.   Lupski, J.R., et al. 1991. DNA duplication associated with Charcot-Marie-Tooth

580   disease type 1A. *Cell* 66:219-232.

581 4.   Matsunami, N., et al. 1992. Peripheral myelin protein-22 gene maps in the duplication

582   in chromosome 17p11.2 associated with Charcot-Marie-Tooth 1A. *Nat Genet* 1:176-

583   179.

584 5.   Patel, P.I., et al. 1992. The gene for the peripheral myelin protein PMP-22 is a candidate

585   for Charcot-Marie-Tooth disease type 1A. *Nat Genet* 1:159-165.

586   6.   Timmerman, V., et al. 1992. The peripheral myelin protein gene PMP-22 is contained
587   within the Charcot-Marie-Tooth disease type 1A duplication. *Nat Genet* 1:171-175.

588   7.   Valentijn, L.J., et al. 1992. The peripheral myelin gene PMP-22/GAS-3 is duplicated
589   in Charcot-Marie-Tooth disease type 1A. *Nat Genet* 1:166-170.

590   8.   Thomas, P.K., et al. 1997. The phenotypic manifestations of chromosome 17p11.2
591   duplication. *Brain* 120 (Pt 3):465-478.

592   9.   Krajewski, K.M., et al. 2000. Neurological dysfunction and axonal degeneration in
593   Charcot-Marie-Tooth disease type 1A. *Brain* 123 (Pt 7):1516-1527.

594   10.   Snipes, G.J., et al. 1992. Characterization of a novel peripheral nervous system myelin
595   protein (PMP-22/SR13). *J Cell Biol* 117:225-238.

596   11.   Notterpek, L., et al. 2001. Peripheral myelin protein 22 is a constituent of intercellular
597   junctions in epithelia. *Proc Natl Acad Sci U S A* 98:14404-14409.

598   12.   Adlkofer, K., et al. 1995. Hypermyelination and demyelinating peripheral neuropathy
599   in Pmp22-deficient mice. *Nat Genet* 11:274-280.

600   13.   Adlkofer, K., et al. 1997. Heterozygous peripheral myelin protein 22-deficient mice are
601   affected by a progressive demyelinating tomaculous neuropathy. *J Neurosci* 17:4662-
602   4671.

603   14.   Suh, J.G., et al. 1997. An in-frame deletion in peripheral myelin protein-22 gene causes
604   hypomyelination and cell death of the Schwann cells in the new Trembler mutant mice.
605   *Neuroscience* 79:735-744.

606   15.   Fledrich, R., et al. 2014. Soluble neuregulin-1 modulates disease pathogenesis in rodent
607   models of Charcot-Marie-Tooth disease 1A. *Nat Med* 20:1055-1061.

608   16.   Roa, B.B., et al. 1993. Molecular basis of Charcot-Marie-Tooth disease type 1A: gene
609   dosage as a novel mechanism for a common autosomal dominant condition. *Am J Med*
610   *Sci* 306:177-184.

611   17.   Yoshikawa, H., et al. 1994. Elevated expression of messenger RNA for peripheral

612   myelin protein 22 in biopsied peripheral nerves of patients with Charcot-Marie-Tooth

613   disease type 1A. *Ann Neurol* 35:445-450.

614   18.   Vallat, J.M., et al. 1996. Ultrastructural PMP22 expression in inherited demyelinating

615   neuropathies. *Ann Neurol* 39:813-817.

616   19.   Svaren, J., et al. 2019. Schwann cell transcript biomarkers for hereditary neuropathy

617   skin biopsies. *Ann Neurol* 85:887-898.

618   20.   Sereda, M., et al. 1996. A transgenic rat model of Charcot-Marie-Tooth disease. *Neuron*

619   16:1049-1060.

620   21.   Huxley, C., et al. 1996. Construction of a mouse model of Charcot-Marie-Tooth disease

621   type 1A by pronuclear injection of human YAC DNA. *Hum Mol Genet* 5:563-569.

622   22.   Huxley, C., et al. 1998. Correlation between varying levels of PMP22 expression and

623   the degree of demyelination and reduction in nerve conduction velocity in transgenic

624   mice. *Hum Mol Genet* 7:449-458.

625   23.   Robertson, A.M., et al. 1999. Development of early postnatal peripheral nerve

626   abnormalities in Trembler-J and PMP22 transgenic mice. *J Anat* 195 (Pt 3):331-339.

627   24.   Norreel, J.C., et al. 2001. Behavioural profiling of a murine Charcot-Marie-Tooth

628   disease type 1A model. *Eur J Neurosci* 13:1625-1634.

629   25.   Robaglia-Schlupp, A., et al. 2002. PMP22 overexpression causes dysmyelination in

630   mice. *Brain* 125:2213-2221.

631   26.   Sereda, M.W., et al. 2006. Animal models of Charcot-Marie-Tooth disease type 1A.

632   *Neuromolecular Med* 8:205-216.

633   27.   Verhamme, C., et al. 2011. Myelin and axon pathology in a long-term study of PMP22-

634   overexpressing mice. *J Neuropathol Exp Neurol* 70:386-398.

635   28.   Fledrich, R., et al. 2012. Murine therapeutic models for Charcot-Marie-Tooth (CMT)

636   disease. *Br Med Bull* 102:89-113.

637   29.   Jouaud, M., et al. 2019. Rodent models with expression of PMP22: Relevance to

638   dysmyelinating CMT and HNPP. *J Neurol Sci* 398:79-90.

639   30.   Bosco, L., et al. 2021. Animal Models as a Tool to Design Therapeutical Strategies for

640   CMT-like Hereditary Neuropathies. *Brain Sci* 11.

641   31.   Pareek, S., et al. 1997. Neurons promote the translocation of peripheral myelin protein

642   22 into myelin. *J Neurosci* 17:7754-7762.

643   32.   Notterpek, L., et al. 1999. PMP22 accumulation in aggresomes: implications for

644   CMT1A pathology. *Neurobiol Dis* 6:450-460.

645   33.   Ryan, M.C., et al. 2002. Aggresome formation in neuropathy models based on

646   peripheral myelin protein 22 mutations. *Neurobiol Dis* 10:109-118.

647   34.   Fortun, J., et al. 2005. Impaired proteasome activity and accumulation of ubiquitinated

648   substrates in a hereditary neuropathy model. *J Neurochem* 92:1531-1541.

649   35.   Sahenk, Z., et al. 2005. NT-3 promotes nerve regeneration and sensory improvement in

650   CMT1A mouse models and in patients. *Neurology* 65:681-689.

651   36.   Sahenk, Z., et al. 2014. AAV1.NT-3 gene therapy for charcot-marie-tooth neuropathy.

652   *Mol Ther* 22:511-521.

653   37.   Sahenk, Z., et al. 2020. Gene therapy to promote regeneration in Charcot-Marie-Tooth

654   disease. *Brain Res* 1727:146533.

655   38.   Khajavi, M., et al. 2007. Oral curcumin mitigates the clinical and neuropathologic

656   phenotype of the Trembler-J mouse: a potential therapy for inherited neuropathy. *Am J

657   Hum Genet* 81:438-453.

658   39.   Meyer zu Horste, G., et al. 2007. Antiprogesterone therapy uncouples axonal loss from

659   demyelination in a transgenic rat model of CMT1A neuropathy. *Ann Neurol* 61:61-72.

660   40.   Verhamme, C., et al. 2009. Oral high dose ascorbic acid treatment for one year in young

661   CMT1A patients: a randomised, double-blind, placebo-controlled phase II trial. *BMC*

662   *Med* 7:70.

663   41.   Madorsky, I., et al. 2009. Intermittent fasting alleviates the neuropathic phenotype in a

664   mouse model of Charcot-Marie-Tooth disease. *Neurobiol Dis* 34:146-154.

665   42.   Nobbio, L., et al. 2009. P2X7-mediated increased intracellular calcium causes

666   functional derangement in Schwann cells from rats with CMT1A neuropathy. *J Biol*

667   *Chem* 284:23146-23158.

668   43.   Rangaraju, S., et al. 2010. Rapamycin activates autophagy and improves myelination

669   in explant cultures from neuropathic mice. *J Neurosci* 30:11388-11397.

670   44.   Chahbouni, M., et al. 2010. Melatonin treatment normalizes plasma pro-inflammatory

671   cytokines and nitrosative/oxidative stress in patients suffering from Duchenne muscular

672   dystrophy. *J Pineal Res* 48:282-289.

673   45.   Pareyson, D., et al. 2011. Ascorbic acid in Charcot-Marie-Tooth disease type 1A

674   (CMT-TRIAAL and CMT-TRAUK): a double-blind randomised trial. *Lancet Neurol*

675   10:320-328.

676   46.   Kullenberg, D., et al. 2012. Health effects of dietary phospholipids. *Lipids Health Dis*

677   11:3.

678   47.   Attarian, S., et al. 2014. An exploratory randomised double-blind and placebo-

679   controlled phase 2 study of a combination of baclofen, naltrexone and sorbitol

680   (PXT3003) in patients with Charcot-Marie-Tooth disease type 1A. *Orphanet J Rare*

681   *Dis* 9:199.

682   48.   Chumakov, I., et al. 2014. Polytherapy with a combination of three repurposed drugs

683   (PXT3003) down-regulates Pmp22 over-expression and improves myelination, axonal

684   and functional parameters in models of CMT1A neuropathy. *Orphanet J Rare Dis*

685   9:201.

686 49. Nicks, J., et al. 2014. Rapamycin improves peripheral nerve myelination while it fails

687   to benefit neuromuscular performance in neuropathic mice. *Neurobiol Dis* 70:224-236.

688 50. Hantke, J., et al. 2014. c-Jun activation in Schwann cells protects against loss of sensory

689   axons in inherited neuropathy. *Brain* 137:2922-2937.

690 51. Ndong   Ntoutoume,   G.M.A.,   et   al.   2016.   Development   of   curcumin-

691   cyclodextrin/cellulose nanocrystals complexes: New anticancer drug delivery systems.

692   *Bioorg Med Chem Lett* 26:941-945.

693 52. Kiepura, A.J., et al. 2018. CharcotMarieTooth type 1A drug therapies: role of adenylyl

694   cyclase activity and Gprotein coupled receptors in disease pathomechanism. *Acta*

695   *Neurobiol Exp (Wars)* 78:198-209.

696 53. Fledrich, R., et al. 2018. Targeting myelin lipid metabolism as a potential therapeutic

697   strategy in a model of CMT1A neuropathy. *Nat Commun* 9:3025.

698 54. Prukop, T., et al. 2019. Early short-term PXT3003 combinational therapy delays

699   disease onset in a transgenic rat model of Charcot-Marie-Tooth disease 1A (CMT1A).

700   *PLoS One* 14:e0209752.

701 55. Fledrich, R., et al. 2019. NRG1 type I dependent autoparacrine stimulation of Schwann

702   cells in onion bulbs of peripheral neuropathies. *Nat Commun* 10:1840.

703 56. Prukop, T., et al. 2020. Synergistic PXT3003 therapy uncouples neuromuscular

704   function from dysmyelination in male Charcot-Marie-Tooth disease type 1A (CMT1A)

705   rats. *J Neurosci Res* 98:1933-1952.

706 57. Ha, N., et al. 2020. A novel histone deacetylase 6 inhibitor improves myelination of

707   Schwann cells in a model of Charcot-Marie-Tooth disease type 1A. *Br J Pharmacol*

708   177:5096-5113.

709 58.   Caillaud, M., et al. 2020. Curcumin-cyclodextrin/cellulose nanocrystals improve the

710   phenotype of Charcot-Marie-Tooth-1A transgenic rats through the reduction of

711   oxidative stress. *Free Radic Biol Med* 161:246-262.

712 59.   Park, N.Y., et al. 2021. Farnesol Ameliorates Demyelinating Phenotype in a Cellular

713   and Animal Model of Charcot-Marie-Tooth Disease Type 1A. *Curr Issues Mol Biol*

714   43:2011-2021.

715 60.   Attarian, S., et al. 2021. A double-blind, placebo-controlled, randomized trial of

716   PXT3003 for the treatment of Charcot-Marie-Tooth type 1A. *Orphanet J Rare Dis*

717   16:433.

718 61.   Stavrou, M., et al. 2021. Emerging Therapies for Charcot-Marie-Tooth Inherited

719   Neuropathies. *Int J Mol Sci* 22.

720 62.   Martinez, N.J., et al. 2021. Genome-Edited Coincidence and PMP22-HiBiT Fusion

721   Reporter Cell Lines Enable an Artifact-Suppressive Quantitative High-Throughput

722   Screening Strategy for PMP22 Gene-Dosage Disorder Drug Discovery. *ACS*

723   *Pharmacol Transl Sci* 4:1422-1436.

724 63.   Lee, J.S., et al. 2020. Targeted PMP22 TATA-box editing by CRISPR/Cas9 reduces

725   demyelinating neuropathy of Charcot-Marie-Tooth disease type 1A in mice. *Nucleic*

726   *Acids Res* 48:130-140.

727 64.   Hai, M., et al. 2001. Competitive binding of triplex-forming oligonucleotides in the two

728   alternate promoters of the PMP22 gene. *Antisense Nucleic Acid Drug Dev* 11:233-246.

729 65.   Lee, J.S., et al. 2017. Pmp22 mutant allele-specific siRNA alleviates demyelinating

730   neuropathic phenotype in vivo. *Neurobiol Dis* 100:99-107.

731 66.   Zhao, H.T., et al. 2018. PMP22 antisense oligonucleotides reverse Charcot-Marie-

732   Tooth disease type 1A features in rodent models. *J Clin Invest* 128:359-368.

733   67.   Boutary, S., et al. 2021. Squalenoyl siRNA PMP22 nanoparticles are effective in
734   treating mouse models of Charcot-Marie-Tooth disease type 1 A. *Commun Biol* 4:317.

735   68.   Boutary, S., et al. 2021. Treating PMP22 gene duplication-related Charcot-Marie-Tooth
736   disease: the past, the present and the future. *Transl Res* 227:100-111.

737   69.   Carrington, J.C., et al. 2003. Role of microRNAs in plant and animal development.
738   *Science* 301:336-338.

739   70.   He, L., et al. 2004. MicroRNAs: small RNAs with a big role in gene regulation. *Nat*
740   *Rev Genet* 5:522-531.

741   71.   Serfecz, J., et al. 2019. Downregulation of the human peripheral myelin protein 22 gene
742   by miR-29a in cellular models of Charcot-Marie-Tooth disease. *Gene Ther* 26:455-464.

743   72.   Lee, J.S., et al. 2019. miR-381 Attenuates Peripheral Neuropathic Phenotype Caused
744   by Overexpression of PMP22. *Exp Neurobiol* 28:279-288.

745   73.   Gautier, B., et al. 2021. AAV2/9-mediated silencing of PMP22 prevents the
746   development of pathological features in a rat model of Charcot-Marie-Tooth disease 1
747   A. *Nat Commun* 12:2356.

748   74.   Boudreau, R.L., Garwick-Coppens, S. E., Liu, J., Wallace, L. M., Harper, S. Q. 2011.
749   Rapid Cloning and Validation of MicroRNA Shuttle Vectors: A Practical Guide. In *In*
750   *RNA Interference Technique*: Humana Springer Press. 19-37.

751   75.   Wallace, L.M., et al. 2018. Pre-clinical Safety and Off-Target Studies to Support
752   Translation of AAV-Mediated RNAi Therapy for FSHD. *Mol Ther Methods Clin Dev*
753   8:121-130.

754   76.   Schiza, N., et al. 2019. Gene replacement therapy in a model of Charcot-Marie-Tooth
755   4C neuropathy. *Brain* 142:1227-1241.

756   77.   Kagiava, A., et al. 2019. Gene replacement therapy after neuropathy onset provides
757   therapeutic benefit in a model of CMT1X. *Hum Mol Genet* 28:3528-3542.

758   78.   Kagiava, A., et al. 2021. AAV9-mediated Schwann cell-targeted gene therapy rescues

759   a model of demyelinating neuropathy. *Gene Ther* 28:659-675.

760   79.   Rossor, A.M., et al. 2021. A longitudinal and cross-sectional study of plasma

761   neurofilament light chain concentration in Charcot-Marie-Tooth disease. *J Peripher*

762   *Nerv Syst*.

763   80.   Jeon, H., et al. 2022. Cytokines secreted by mesenchymal stem cells reduce

764   demyelination in an animal model of Charcot-Marie-Tooth disease. *Biochem Biophys*

765   *Res Commun* 597:1-7.

766   81.   Jennings, M.J., et al. 2022. NCAM1 and GDF15 are biomarkers of Charcot-Marie-

767   Tooth disease in patients and mice. *Brain*.

768   82.   Kao, M.L., et al. 2020. Pharmacokinetics and distribution of 2-hydroxypropyl-beta-

769   cyclodextrin following a single intrathecal dose to cats. *J Inherit Metab Dis* 43:618-

770   634.

771   83.   Bradbury, A.M., et al. 2020. Krabbe disease successfully treated via monotherapy of

772   intrathecal gene therapy. *J Clin Invest* 130:4906-4920.

773   84.   Kagiava, A., et al. 2021. Efficacy of AAV serotypes to target Schwann cells after

774   intrathecal and intravenous delivery. *Sci Rep* 11:23358.

775   85.   Berciano, J., et al. 2000. Clinico-electrophysiological correlation of extensor digitorum

776   brevis muscle atrophy in children with charcot-marie-tooth disease 1A duplication.

777   *Neuromuscul Disord* 10:419-424.

778   86.   Burns, J., et al. 2009. Evolution of foot and ankle manifestations in children with

779   CMT1A. *Muscle Nerve* 39:158-166.

780   87.   Verhamme, C., et al. 2004. Clinical disease severity and axonal dysfunction in

781   hereditary motor and sensory neuropathy Ia. *J Neurol* 251:1491-1497.

782   88.   Manganelli, F., et al. 2016. Nerve conduction velocity in CMT1A: what else can we

783   tell? *Eur J Neurol* 23:1566-1571.

784   89.   Perea, J., et al. 2001. Induced myelination and demyelination in a conditional mouse

785   model of Charcot-Marie-Tooth disease type 1A. *Hum Mol Genet* 10:1007-1018.

786   90.   Maier, M., et al. 2003. Distinct elements of the peripheral myelin protein 22 (PMP22)

787   promoter regulate expression in Schwann cells and sensory neurons. *Mol Cell Neurosci*

788   24:803-817.

789   91.   Roux, K.J., et al. 2004. The temporospatial expression of peripheral myelin protein 22

790   at the developing blood-nerve and blood-brain barriers. *J Comp Neurol* 474:578-588.

791   92.   Stavrou, M., et al. 2021. Genetic mechanisms of peripheral nerve disease. *Neurosci Lett*

792   742:135357.

793   93.   Naveed, A., et al. 2021. Onasemnogene Abeparvovec (AVXS-101) for the Treatment

794   of Spinal Muscular Atrophy. *J Pediatr Pharmacol Ther* 26:437-444.

795   94.   Bailey, R.M., et al. 2018. Development of Intrathecal AAV9 Gene Therapy for Giant

796   Axonal Neuropathy. *Mol Ther Methods Clin Dev* 9:160-171.

797   95.   Sancho, S., et al. 1999. Distal axonopathy in peripheral nerves of PMP22-mutant mice.

798   *Brain* 122 (Pt 8):1563-1577.

799   96.   Jeng, C.L., et al. 2011. Intraneural injections and regional anesthesia: the known and

800   the unknown. *Minerva Anestesiol* 77:54-58.

801   97.   Meyer, K., et al. 2015. Improving single injection CSF delivery of AAV9-mediated

802   gene therapy for SMA: a dose-response study in mice and nonhuman primates. *Mol*

803   *Ther* 23:477-487.

804   98.   Mendell, J.R., et al. 2017. Single-Dose Gene-Replacement Therapy for Spinal

805   Muscular Atrophy. *N Engl J Med* 377:1713-1722.

806   99.   Al-Zaidy, S.A., et al. 2019. From Clinical Trials to Clinical Practice: Practical

807   Considerations for Gene Replacement Therapy in SMA Type 1. *Pediatr Neurol* 100:3-

808   11.

809   100. Van Alstyne, M., et al. 2021. Gain of toxic function by long-term AAV9-mediated

810   SMN overexpression in the sensorimotor circuit. *Nat Neurosci* 24:930-940.

811   101. Keiser, M.S., et al. 2021. Toxicity after AAV delivery of RNAi expression constructs

812   into nonhuman primate brain. *Nat Med* 27:1982-1989.

813   102. Hordeaux, J., et al. 2020. Adeno-Associated Virus-Induced Dorsal Root Ganglion

814   Pathology. *Hum Gene Ther* 31:808-818.

815   103. de Visser, M., et al. 2011. Ascorbic acid for treatment in CMT1A: what's next? *Lancet

816   Neurol* 10:291-293.

817   104. Bren, L. 2006. The importance of patient-reported outcomes...it's all about the patients.

818   *FDA Consum* 40:26-32.

819   105. Menotti, F., et al. 2014. Amount and intensity of daily living activities in Charcot-

820   Marie-Tooth 1A patients. *Brain Behav* 4:14-20.

821   106. Padua, L., et al. 2016. Novel outcome measures for Charcot-Marie-Tooth disease:

822   validation and reliability of the 6-min walk test and StepWatch() Activity Monitor and

823   identification of the walking features related to higher quality of life. *Eur J Neurol*

824   23:1343-1350.

825   107. Johnson, N.E., et al. 2018. The Charcot-Marie-Tooth Health Index: Evaluation of a

826   Patient-Reported Outcome. *Ann Neurol* 84:225-233.

827   108. Morrow, J.M., et al. 2018. Validation of MRC Centre MRI calf muscle fat fraction

828   protocol as an outcome measure in CMT1A. *Neurology* 91:e1125-e1129.

829   109. Sandelius, A., et al. 2018. Plasma neurofilament light chain concentration in the

830   inherited peripheral neuropathies. *Neurology* 90:e518-e524.

831   110.   Millere, E., et al. 2021. Plasma neurofilament light chain as a potential biomarker in

832   Charcot-Marie-Tooth disease. *Eur J Neurol* 28:974-981.

833   111.   Fledrich, R., et al. 2017. Biomarkers predict outcome in Charcot-Marie-Tooth disease

834   1A. *J Neurol Neurosurg Psychiatry* 88:941-952.

835   112.   Wang, D., et al. 2019. Adeno-associated virus vector as a platform for gene therapy

836   delivery. *Nat Rev Drug Discov* 18:358-378.

837   113.   Visigalli, D., et al. 2020. Exploiting Sphingo- and Glycerophospholipid Impairment to

838   Select Effective Drugs and Biomarkers for CMT1A. *Front Neurol* 11:903.

839 **FIGURES**
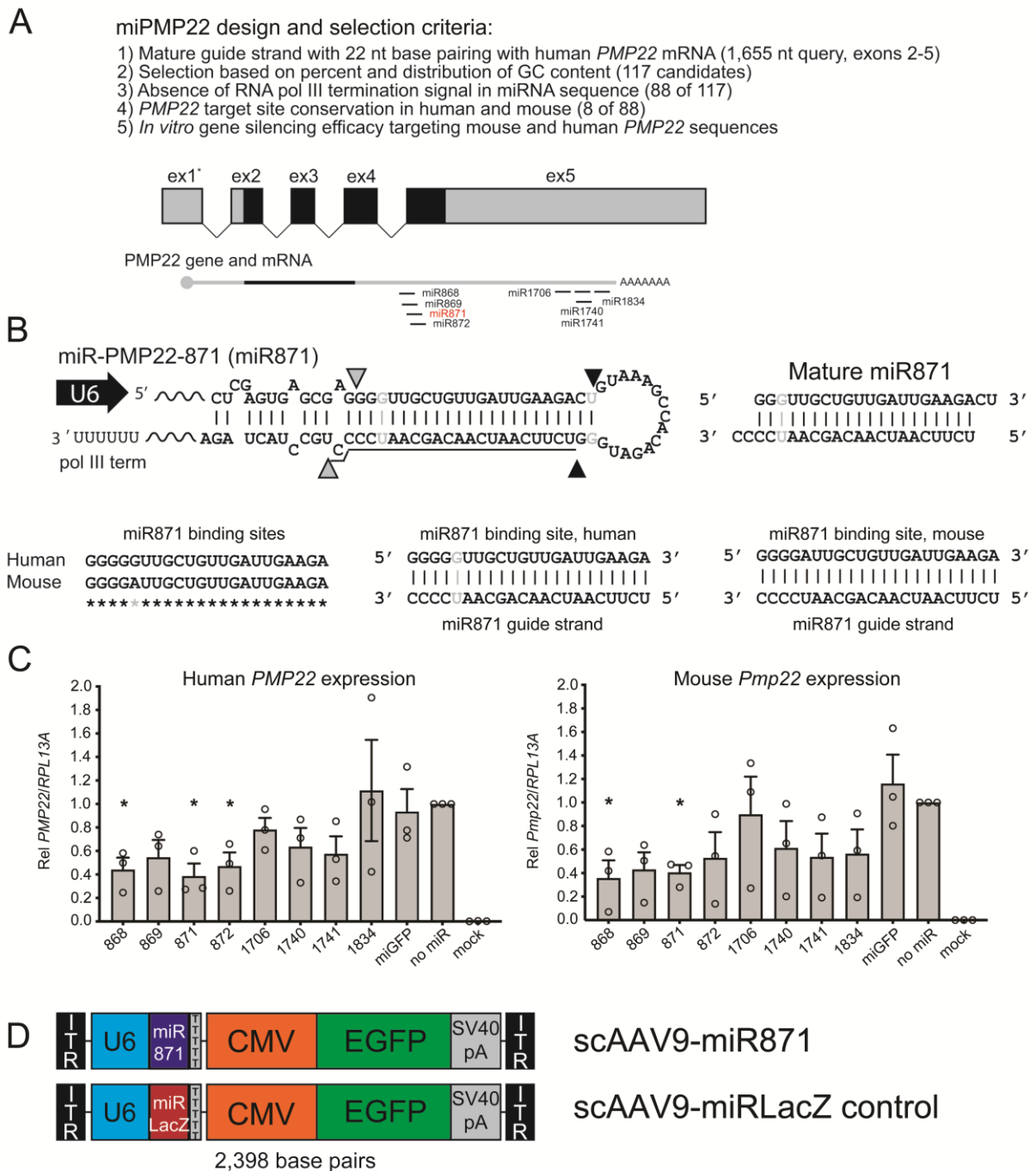
841 **Figure 1. Design and *in vitro* screen of artificial microRNAs targeting PMP22**. **(A)** Full-length *PMP22*

842 mRNA is transcribed from 5 exons, producing 2 major transcripts with identical ORFs (black shading). We

843 designed 8 candidates miRNAs to equally target both human *PMP22* and mouse *Pmp22* mRNAs. **(B)** Grey and

844 black arrowheads show miR871 cut sites by Drosha and Dicer, respectively. Double-stranded RNAs form G:U

845 wobble base pairs (indicated by grey shading). Underlined sequence represents the mature miR871 antisense guide

846 strand. Bottom shows alignment of the miR871 binding site on human and mouse *PMP22/Pmp22* mRNA. Grey

847   asterisk indicates a G:A mismatch at the miR871 binding site, but each nucleotide at this location can form two

848   hydrogen bonds with the miR871 guide strand as a G:U wobble (human) or A:U (mouse). **(C)** RT-qPCR to

849   measure *in vitro* human *PMP22* or mouse *Pmp22* silencing by indicated miRPMP22s (n=3/group). Gene

850   expression was normalized to human *RPL13A*. Data were compared using unpaired t-test. Values represent mean

851   ± SEM. **(D)** Schematic of scAAV9 used to deliver miR871 or miRLacZ expression cassettes *in vivo*. U6 promoter

852   drives transcription of miR871 or miRLacZ and CMV promoter drives EGFP gene with SV40 polyadenylation

853   sequence.
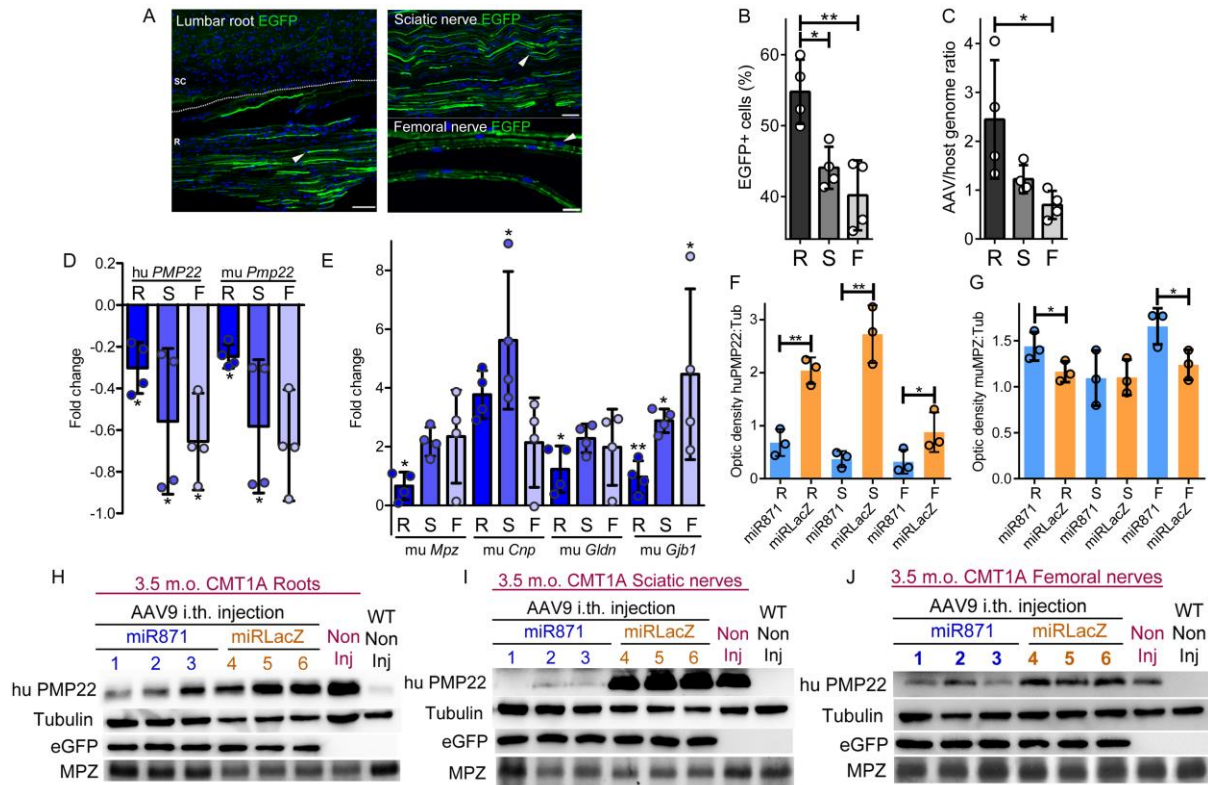
Figure 2. *In vivo* assessment of AAV9-miR transduction in PNS tissues and validation of AAV9-miR871 silencing efficiency in a CMT1A mouse model at 6 weeks post injection. (A) Lumbar spinal roots and sciatic nerve sections, as well as teased femoral nerve fibers showing EGFP autofluorescence in SCs and axons. Arrowheads indicate example of EGFP+ nuclei. **(B)** Quantification of EGFP-expressing PNS cells (n=4/group). **(C)** VGCN (n=4/group) confirm peripheral nerves transduction. RT-qPCR analysis of **(D)** hu*PMP22* and mu*Pmp22* and of **(E)** mu*Mpz*, mu*Cnp*, mu*Gldn* and mu*Gjb1* gene expression (n=3/group). Fold relative mRNA expression levels of CMT1A-AAV9-miR871 were calculated compared to CMT1A-AAV9-miRLacZ mice. All samples were normalized to endogenous *Gapdh*. Quantification of **(F)** huPMP22 and **(G)** muMPZ western blot protein optical densities, normalized to tubulin, in CMT1A-AAV9-miR871 and CMT1A-AAV9-miRLacZ mice in lumbar roots (R), sciatic (S) and femoral (F) nerves. Western blot showing huPMP22, muTubulin, EGFP and muMPZ protein levels in **(H)** roots, **(I)** sciatic and **(J)** femoral nerves**.** Values represent mean ± SD. Data were compared using One-way ANOVA with Tukey's Multiple Comparison Test. Significance level for all comparisons, P<0.05. Scale bars: **(A)** Lumbar root & sciatic nerve: 60 μm, femoral nerve: 20 μm.

868
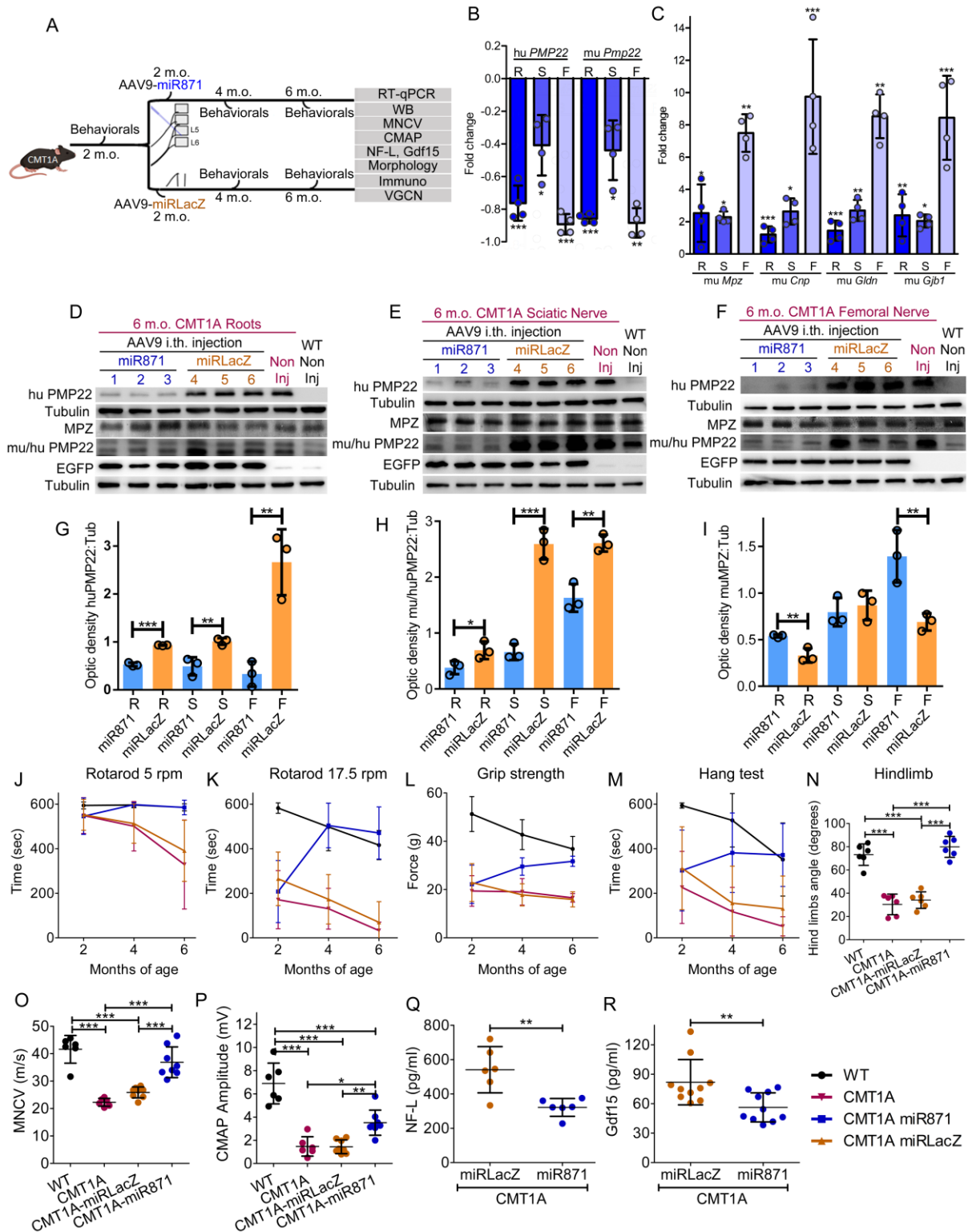
Figure 3. Efficient *PMP22/Pmp22* silencing and improvement of motor behavioral, electrophysiological and blood biomarker phenotypes following early treatment of CMT1A mice. (A) Design of the early treatment trial. RT-qPCR analysis of **(B)** hu*PMP22* and mu*Pmp22* and **(C)** mu*Mpz*, mu*Cnp*, mu*Gldn* and mu*Gjb1* **(C)** gene expression levels in lumbar roots (R), sciatic (S) and femoral (F) nerves (n=4/group). **(D-I)** Western blot images

40

873   and analysis of huPMP22, muPMP22, muTubulin, EGFP and muMPZ proteins. **(J-M)** Behavioral analysis

874   comparing non-injected WT and CMT1A mice (n=10/group), CMT1A-AAV9-miR871 and CMT1A-AAV9-

875   miRLacZ mice (n=16/group). **(N)** Hindlimbs opening angle estimation in 6-month-old non-injected WT and

876   CMT1A mice (n=6/group) as well as in CMT1A-AAV9-miR871 and CMT1A-AAV9-miRLacZ mice

877   (n=6/group). **(O)** MNCV and **(P)** CMAP analysis in 6-month-old WT and non-injected CMT1A mice

878   (n=6/group), CMT1A-AAV9-miR871 and CMT1A-AAV9-miRLacZ mice (n=8/group). **(Q)** NF-L (n=6/group)

879   and **(R)** Gdf15 (n=10/group) circulating biomarkers analysis in 6-month-old CMT1A-AAV9-miR871 and

880   CMT1A-AAV9-miRLacZ mice. Values represent mean ± SD. For RT-qPCR and circulating biomarkers analysis,

881   comparisons were performed using unpaired t-test. Rest of the data were compared using One-way ANOVA with

882   Tukey's Multiple Comparison Test. Significance level for all comparisons, $P<0.05$.
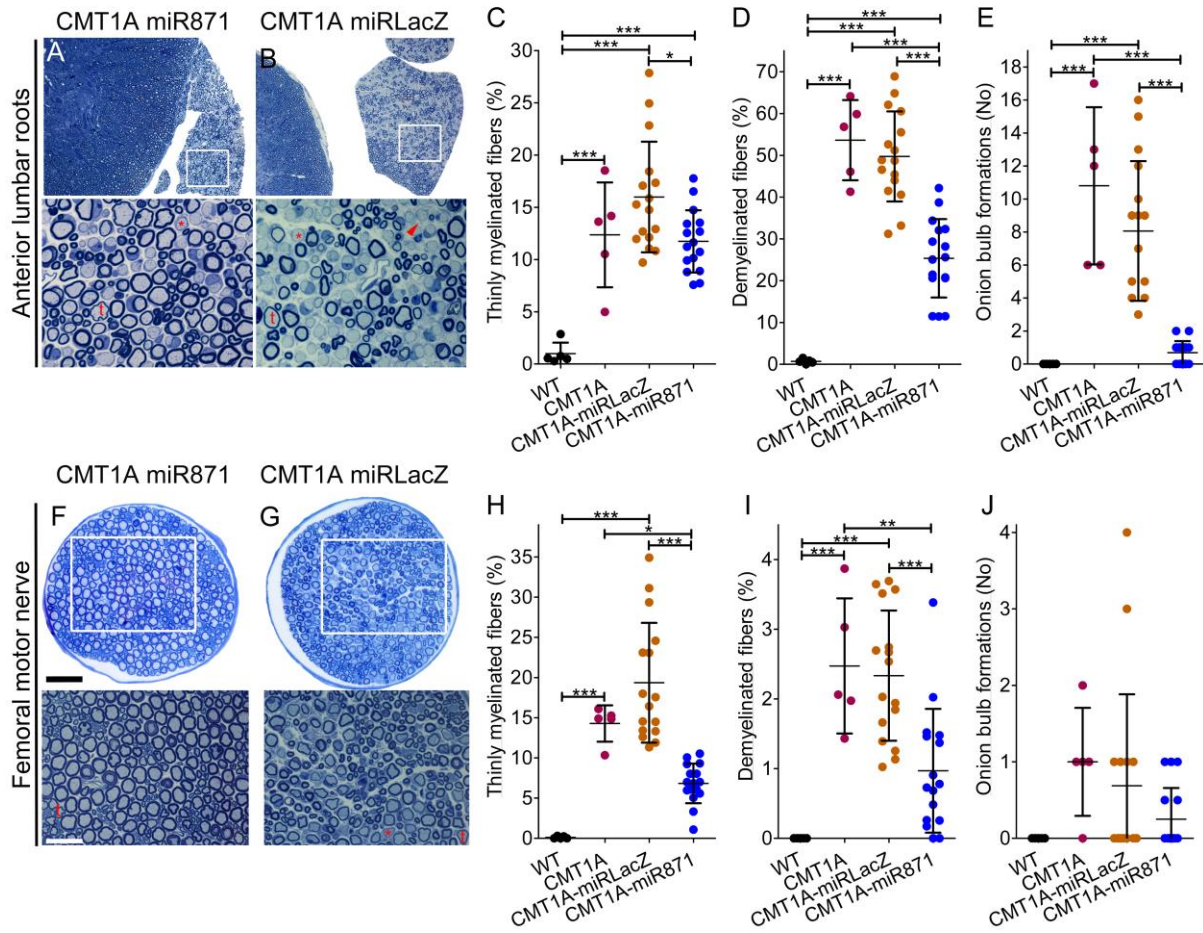
Figure 4. Early treatment of CMT1A mice improved morphology of PNS tissues. Toluidine blue-stained semithin sections of **(A-B)** anterior lumbar spinal roots attached to the spinal cord and **(F-G)** femoral motor nerve at low (upper panels) and higher magnification (lower panels) from CMT1A-AAV9-miR871 and CMT1A-AAV9-miRLacZ mice. Thinly myelinated (t) or demyelinated (*) fibers as well as onion bulb formations (red arrowhead) are indicated. Quantification of abnormally myelinated fibers in **(C-E)** lumbar motor roots and **(H-J)** femoral motor nerves of 6-month-old non-injected WT and CMT1A (n=5/group) mice, as well as in CMT1A-AAV9-miR871 and CMT1A-AAV9-miRLacZ (n=16/group). Values represent mean ± SD. Data were compared using one-way ANOVA with Tukey's Multiple Comparison Test. Significance level for all comparisons, P<0.05. Scale bars: **(A)**: 50 μm, for magnified: 10 μm, **(F)**: 40 μm, for magnified: 25 μm.
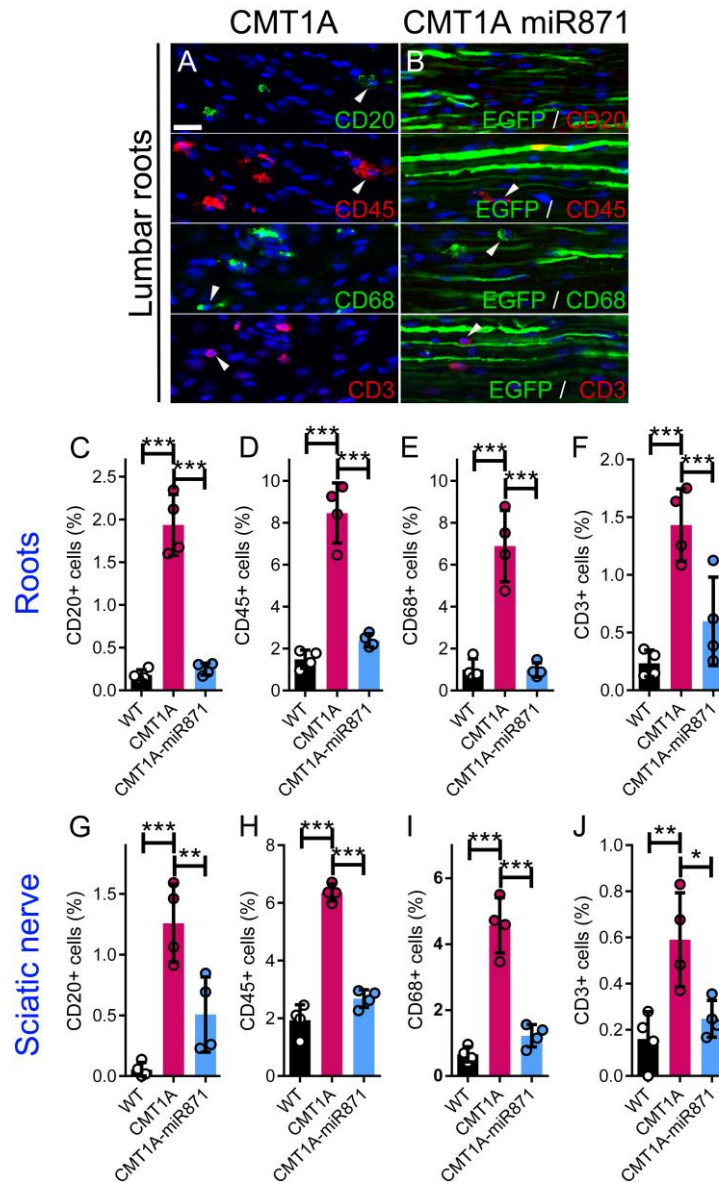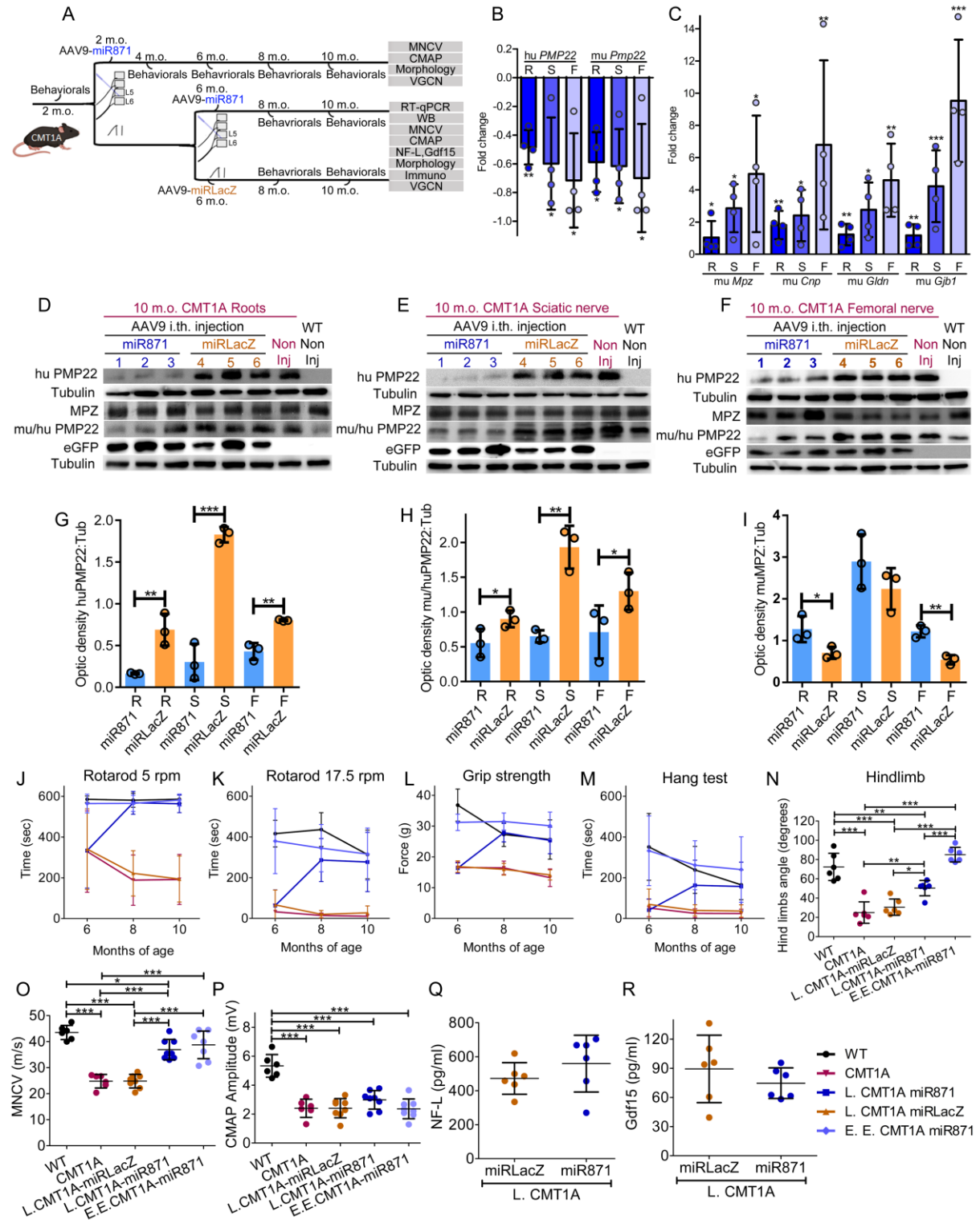
Figure 5. Early treatment of CMT1A mice improved inflammation in PNS tissues. Images of longitudinal lumbar spinal root sections from non-injected and early treated CMT1A-AAV9-miR871 mice immunostained with CD20, CD45, CD68, and CD3 markers (**A, B**), as indicated, (counterstaining with nuclear marker DAPI, blue; EGFP autofluorescence in injected animal tissues). Arrowheads indicate representative CD+ cells. Quantification of the percentage of inflammatory cells in lumbar roots (**C-F**) and sciatic nerve (**G-J**). Values represent mean ± SD (n=4/group). Data were compared using one-way ANOVA with Tukey's Multiple Comparison Test followed by Bonferroni correction. Significance level for all comparisons, $P<0.05$. Scale bar: 20 μm. (WT and CMT1A immunostaining images and quantification data are also shown in Supplemental Figures 8 and 9).

Figure 6. Efficient *PMP22/Pmp22* silencing and improvement of motor function and sciatic MNCV but not of CMAP or blood biomarker phenotypes following late treatment of CMT1A mice. (A) Design of the late (L.) and extended early (E.E.) treatment trial. RT-qPCR analysis of **(B)** hu*PMP22* and mu*Pmp22* and **(C)** mu*Mpz*, mu*Cnp*, mu*Gldn* and mu*Gjb1* gene expression in lumbar roots (R), sciatic (S) and femoral (F) nerves of late-

44

909   treated CMT1A mice (n=4/group). (**D-I**) Western blot images and analysis of huPMP22, muPMP22, muTubulin,

910   eGFP and muMPZ proteins. (**J-M**) Behavioral analysis comparing non-injected WT and CMT1A mice

911   (n=10/group), CMT1A-AAV9-miR871 and CMT1A-AAV9-miRLacZ mice (n=16/group). (**N**) Hindlimbs

912   opening angle estimation in 10-month-old non-injected WT and CMT1A mice (n=6/group), L.CMT1A-AAV9-

913   miR871, E.E.CMT1A-AAV9-miR871 and CMT1A-AAV9-miRLacZ mice (n=6/group). (**O**) MNCV**, (P)** CMAP

914   analysis in 10-month-old WT and non-injected CMT1A mice (n=6/group), L.CMT1A-AAV9-miR871,

915   E.E.CMT1A-AAV9-miR871 and CMT1A-AAV9-miRLacZ mice (n=8/group). (**Q**) NF-L (n=6/group) and (**R**)

916   Gdf15 (n=10/group) circulating biomarkers analysis in 10-month-old L.CMT1A-AAV9-miR871 and L.CMT1A-

917   AAV9-miRLacZ mice. Values represent mean ± SD. For RT-qPCR and circulating biomarkers analysis,

918   comparisons were performed using unpaired t-test. Rest of the data were compared using One-way ANOVA with

919   Tukey's Multiple Comparison Test. Significance level for all comparisons, $P<0.05$.
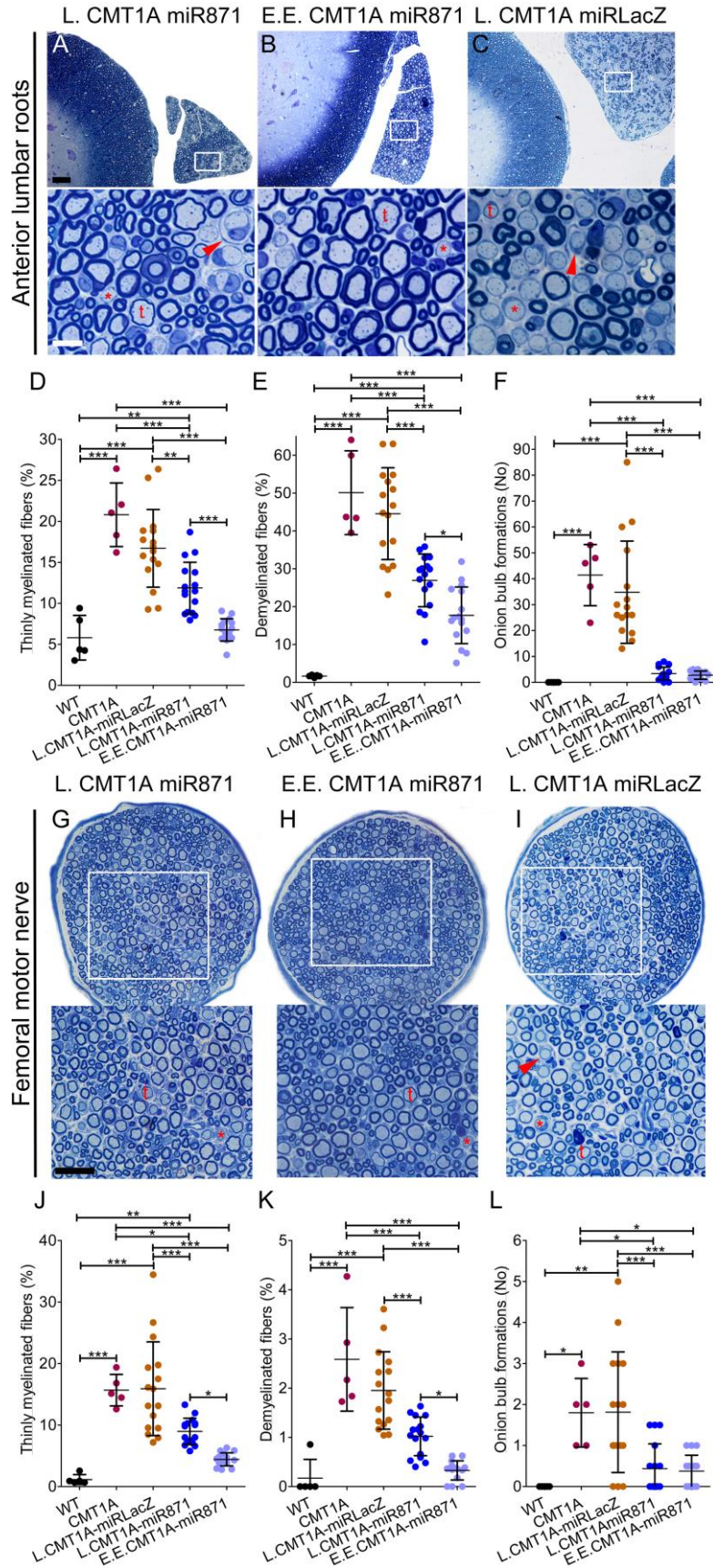
921   **Figure 7. Late and extended early treatment of CMT1A mice improved morphology of PNS tissues.**

922   Toluidine blue-stained semithin sections of **(A-C)** anterior lumbar spinal roots attached to the spinal cord and **(G-**

923   **I)** femoral motor nerves at low and higher magnification from 10-month-old L.CMT1A-AAV9-miR871,

924   E.E.CMT1A-AAV9-miR871 and L.CMT1A-AAV9-miRLacZ mice. Thinly myelinated (t) and demyelinated (*)

925   fibers as well as onion bulb formations (red arrowhead) are indicated. **(D-E)** Quantification of abnormally

926   myelinated fibers in multiple roots and **(J-L)** femoral motor nerves of 10-month-old WT, non-injected CMT1A

927   (n=5/group) mice, L.CMT1A-AAV9-miR871, E.E.CMT1A-AAV9-miR871 and L.CMT1A-AAV9-miRLacZ

928   mice (n=16/group). Values represent mean ± SD. Data were compared using one-way ANOVA with Tukey's

929   Multiple Comparison Test. Significance level for all comparisons, P<0.05. Scale bars: **(A)**: 50 μm, for magnified:

930   10 μm; **(G)**: 40 μm, for magnified: 25 μm.

931
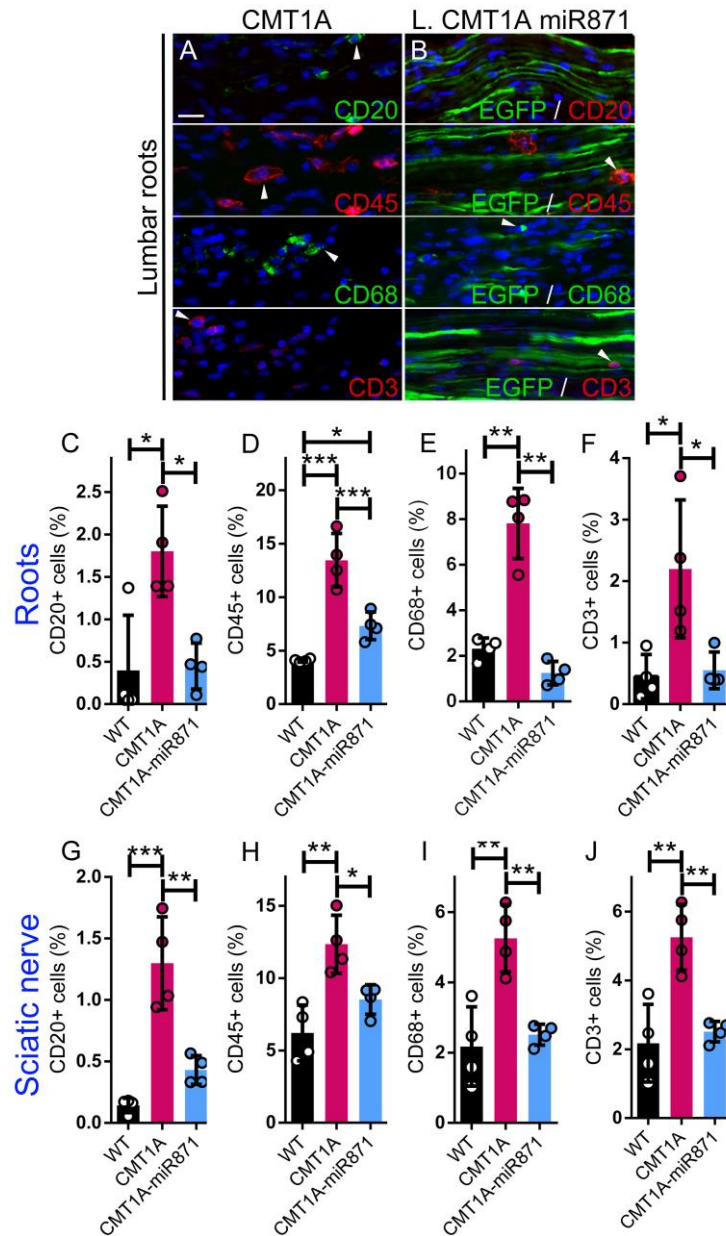
Figure 8. Late treatment of CMT1A mice improved inflammation in PNS tissues. Images of longitudinal lumbar spinal root sections from non-injected and late treated CMT1A-AAV9-miR871 mice immunostained with CD20, CD45, CD68, and CD3 markers **(A, B)**, as indicated, (counterstaining with nuclear marker DAPI, blue; EGFP autofluorescence in injected animal tissues). Arrowheads indicate representative CD+ cells. Quantification of the percentage of inflammatory cells in lumbar roots **(C-F)** and sciatic nerve **(G-J)**. Values represent mean ± SD (n=4/group). Data were compared using one-way ANOVA with Tukey's Multiple Comparison Test. Significance level for all comparisons, $P<0.05$. Scale bar: 20 μm. (Immunostaining images are also shown in Supplemental Figure 25).